CHAPTER V
RESULTS

5.1 Effects of serotonin, dopamine, gonadotropin-releasing hormones, and corazonin, on the androgenic gland of the giant freshwater prawn

In this experiment, it has been hypothesized that serotonin, dopamine, GnRH, and corazonin may have an effect on the AG. So, the prawns were treated by each agent, and then checked with 3 three assay systems: on (1) examination of the external morphology and histology of the AG, ASI index; (2) estimation of AG cell proliferation by BrdU labelling; and (3) quantify the expression the *Mr*IAG by immunohistochemistry, and ELISA.

5.1.1 Morphological and histological changes of the AG

Morphological changes of AG, which is attached to the EB, in each treated group on day 12 were shown in Figure 5.1 (right column). The AG of the prawns treated with 2.5×10^{-6} mol/prawn 5-HT, 500 ng/g BW l-GnRH-III, and 500 ng/g BW oct-GnRH were similar to vehicle control (VC) but larger than the AG of the prawns treated with 2.5×10^{-6} mol/prawn DA, and 500 ng/g BW Crz.

At the same doses, the histological of the cross sections AGs confirm the structure of AGs as shown in Figure 5.1 (left column). The result showed the same trend with external morphology that the AG of the prawns treated with 5-HT and l-GnRH-III were larger than the AG of the prawns treated with VC, DA, and Crz. In contrast, AG of the prawns treated with oct-GnRH was smaller than the VC group.

5.1.2 The AG-somatic index (ASI)

At day 12 and 16 after treatment, the ASI (Figure 5.2) showed the same trend as morphology changes in Figure 5.1. The ASI values of prawns treated with 2.5×10^{-6} mol/prawn 5-HT and 50, 500 ng/g BW l-GnRH-III were significantly higher than the VC (P<0.05). In contrast ASI values of prawns treated with 2.5×10^{-6} and 2.5×10^{-7} mol/prawn DA were significantly lower than the VC (P<0.05). Moreover, ASI values of prawns treated with 50, 500 ng/g BW Crz at day 12 were significantly lower than the VC (P<0.05) but the prawns died before day 16.

5.1.3 Cell proliferation assay using 5-bromo-2'-deoxyuridine (BrdU)

This result showed the dividing cells as having purple nuclei, labeled with BrdU in the AG sections of each group at day 4, 8, 12, and 16 (Figure 5.3, upper panel). The dividing cells of prawns treated with 5-HT and l-GnRH-III were more numerous than the VC, whereas the cells from oct-GnRH-treated group were similar to VC. However, the cells from DA and Crz treated groups, which have 1-2 labeled nuclei in the sections, were less than VC group.

After observing under the microscope, the labeled nuclei of each treated group were quantified, reported in histograms, and compared to VC, which showed nuclei per mm^2 (mean ± S.E.) (Figure 5.3, lower panel). The groups treated with 5-HT and l-GnRH-III showed significantly increased number of labeled nuclei (P<0.05). Moreover, the number of labeled nuclei at the dose of 500 ng/g BW l-GnRH-III appeared to be greatest at D4, whereas the numbers of dividing cells in the two doses of 5-HT appeared to be greatest at D8 (P<0.05). There was a small difference between oct-GnRH and VC group. At 2.5×10^{-6} mol/prawn of DA, the number of labeled nuclei decreased when compared with the VC group (P<0.05). The groups treated with two doses of Crz showed significantly lower numbers of labeled nuclei than the VC (P<0.05), and the prawns had died before day 16.

5.1.4 Specificity of rabbit antiserum against *Mr*IAG (anti-*Mr*IAG)

5.1.4.1 Dot blot analysis

The specificity anti-*Mr*IAG was tested using 1µg/µl of l-GnRH-III, ELH, RPCH, *Mr*IAG synthesis peptide, AG crude extract, and BSA. The two positive dots were shown in *Mr*IAG peptide and the AG extract dots (Figure 5.4, middle row).

5.1.4.2 Expression of r*Mr*IAG protein

After induction by IPTG at 37ºC and 25ºC for three hours, the pro-*Mr*IAG protein was expressed in the induced colony 1 and 4 at both temperature setting (Figures 5.5-5.6). The *rMr*IAG protein size in the bacterial cell lysate was around 20 kDa (black arrowhead).

5.1.4.3 SDS-PAGE and Western blot analysis of *Mr*IAG

The SDS-PAGE analysis showed the bacterial cell lysate proteins, including recombinant *Mr*IAG (*rMr*IAG), and AG extracted proteins (Figure 5.7 A). The *rMr*IAG protein was shown around 17.6 kDa.

The Western blot analysis indicated the immunoreactivity bands between anti-*Mr*IAG and *Mr*IAG protein at 17.6 kDa in both r*Mr*IAG and AG extracts (Figure 5.7 B).

5.1.5 Detection of *Mr*IAG using immunofluorescence

At day 12, the immunofluorescence results showed the immunoreactivity of *Mr*IAG-*ir* in the AG of each group (Figure 5.8). It was shown that *Mr*IAG-*ir* was present throughout the gland but appeared stronger in cells at the edge of the gland in the VC and oct-GnRH-treated groups. Moreover, the *Mr*IAG-*ir* was very intense in cells throughout the gland of the groups treated with 5-HT and l-GnRH-III but very weak in the groups treated with DA and Crz.

5.1.6 Estimation of the relative amounts of *Mr*IAG by ELISA

The relative amounts of *Mr*IAG in each group were quantified by an ELISA assay and the concentration shown as histograms (mean ± S.E.) (Figure 5.9). The relationships of OD's and *Mr*IAG concentrations were quantified using the standard curve (Figure 5.10-5.11). *Mr*IAG concentration in the group treated with 5HT at days 4 and 8 were significantly higher than in the VC group ($P<0.05$). Moreover, at most days of the groups injected with l-GnRH-III and oct-GnRH, *Mr*IAG concentrations were also significantly higher than the VC group ($P<0.05$). However, the concentration of *Mr*IAG of the groups treated with DA and Crz were significantly lower than that of the VC group ($P<0.05$).

In each day of the experiment, the intra-assay coefficient of variations were 3.62%, 5.21%, 5.10%, 3.78% (n = 66), respectively, and inter-assay coefficient of variations were 4.46 % (n = 6) with limit of detection at 0.99 pg/ml (Figure 5.10).

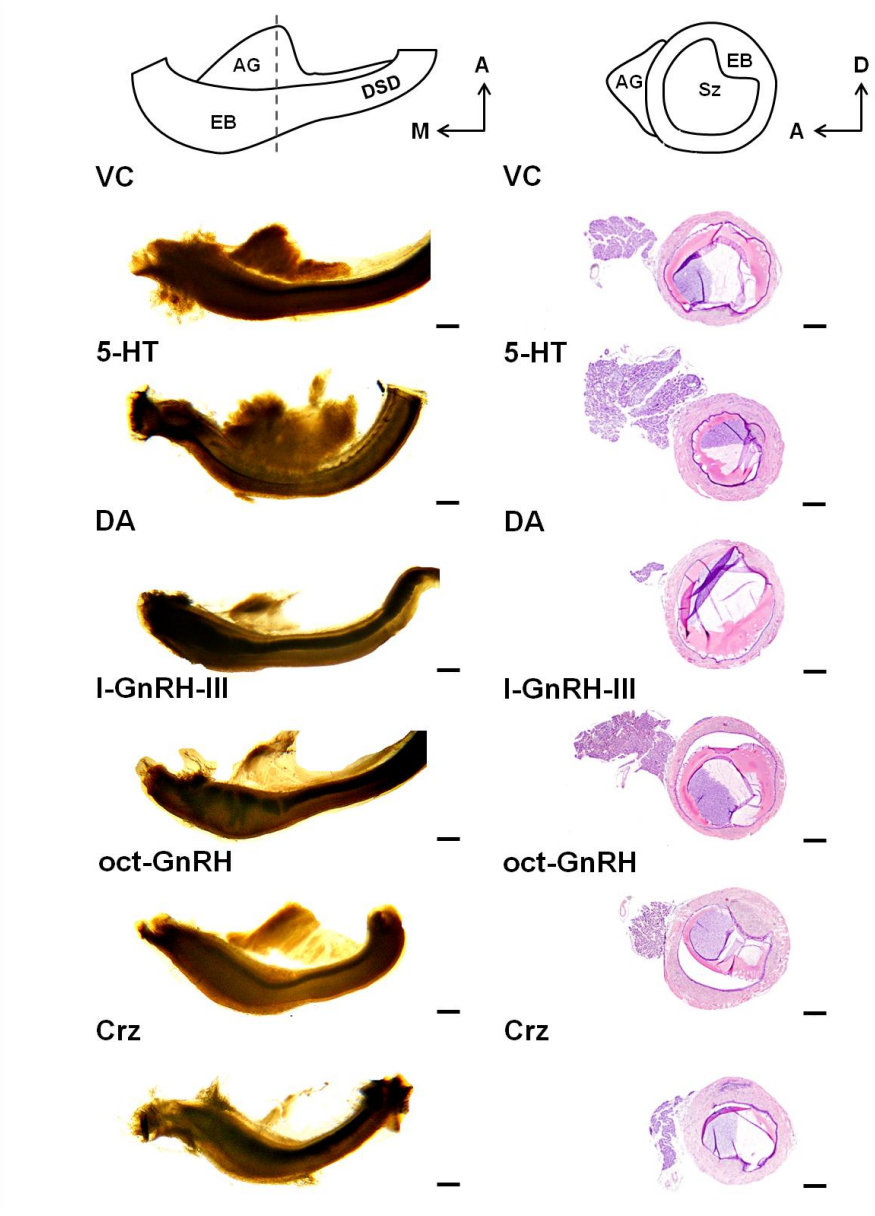

Figure 5.1 External morphology and histology of the AGs of each treated group, including vehicle control (VC) group, 5-HT and DA at a dose of 2.5 x10^{-6} mol/prawn, l-GnRH, oct-GnRH, and Crz at a dose of 500 ng/g BW, at day 12 after treatments. In the left column, dashed line indicates the cross section region for paraffin section (right column). In the right column, the H&E stained showed low power light micrographs of the AG attached to ejaculatory bulb (EB) and spermatic duct (DSD). Sz, spermatozoa; A, anterior; M, medial D, dorsal, Scale bars: left column = 2 mm; middle column = 250 µm.

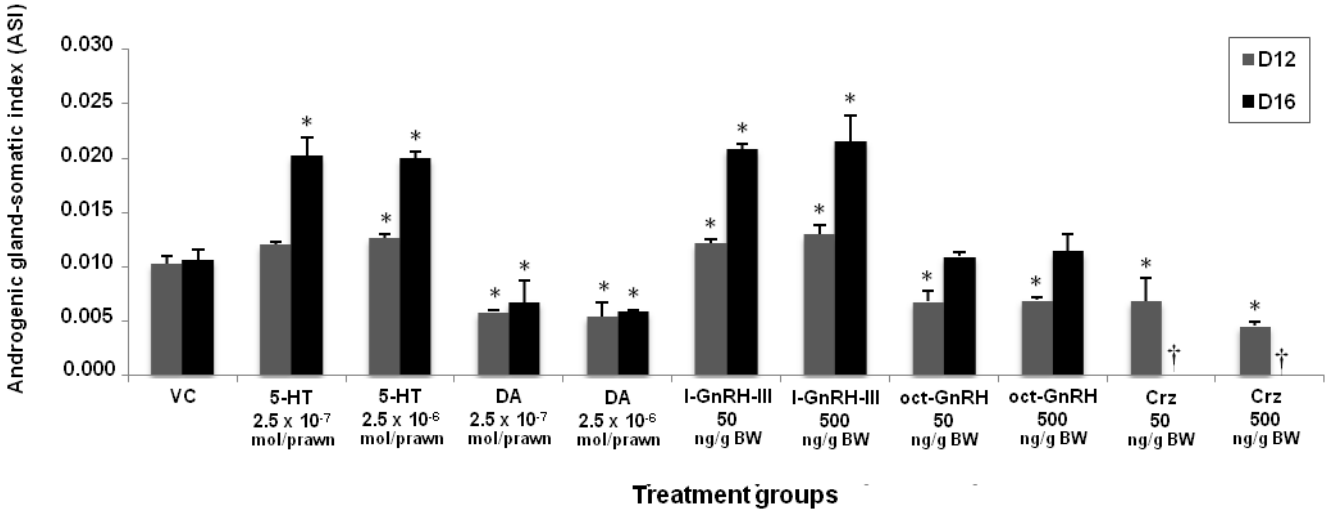

Figure 5.2 Androgenic gland-somatic index (ASI) of each treated group at day 12 and 16, showing significant increases in the groups treated with l-GnRH-III and 5-HT, and significant decreases in the groups treated with DA and Crz when compared with (P<0.05).

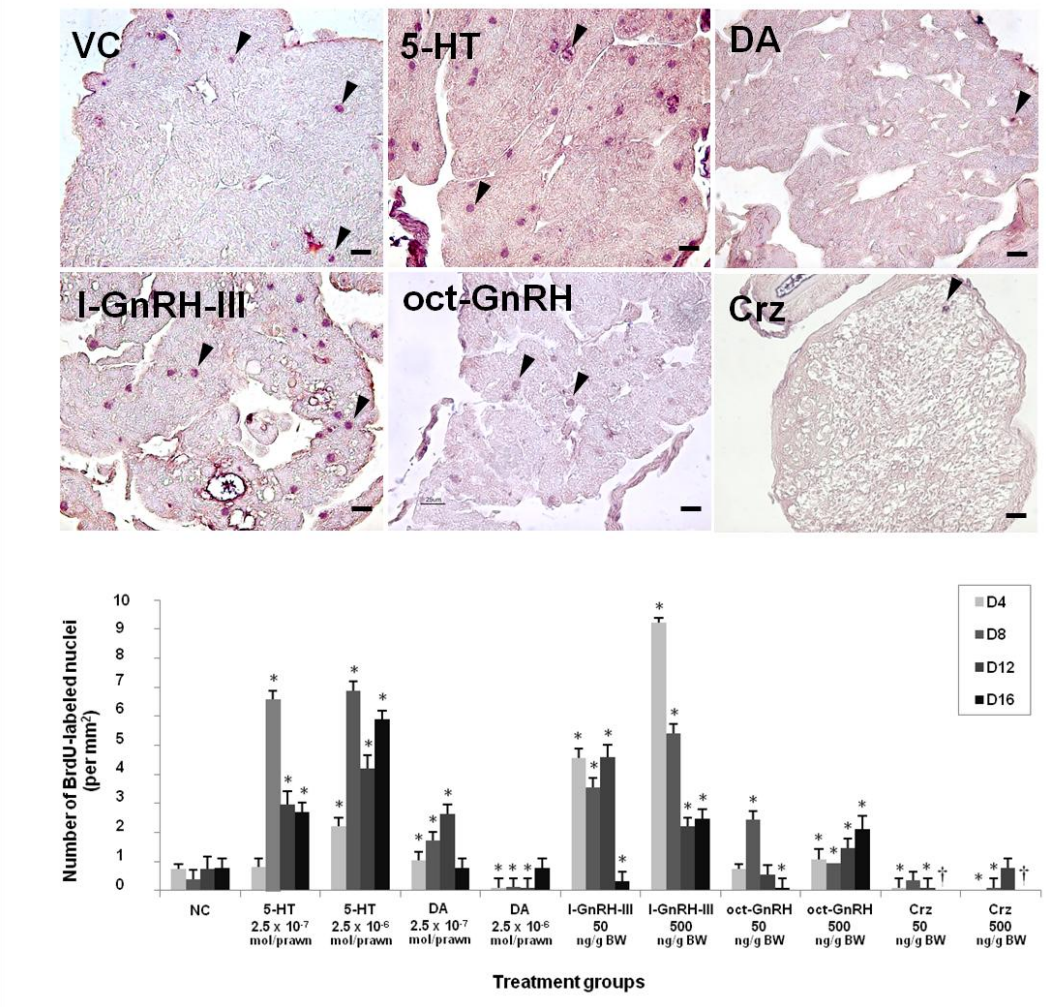

Figure 5.3 BrdU-labeled nuclei showing cell proliferation assay in the AGs at day 4, 8, 12, and 16. BrdU stained at day 12 showing purple dot in the sections indicating proliferative cells (black arrowheads). The greater numbers of BrdU-labeled nuclei are present in the groups treated with 5-HT and l-GnRH-III whereas fewer are present in the groups treated with DA and Crz. Scale bars: left column = 100 µm; right column = 25 µm. Histograms show mean number ± S.E. of BrdU-labeled nuclei per mm^2 area in three sections per prawn (n = 8 animals). *, significant difference from VC (P<0.05); †, prawns died before day 16.

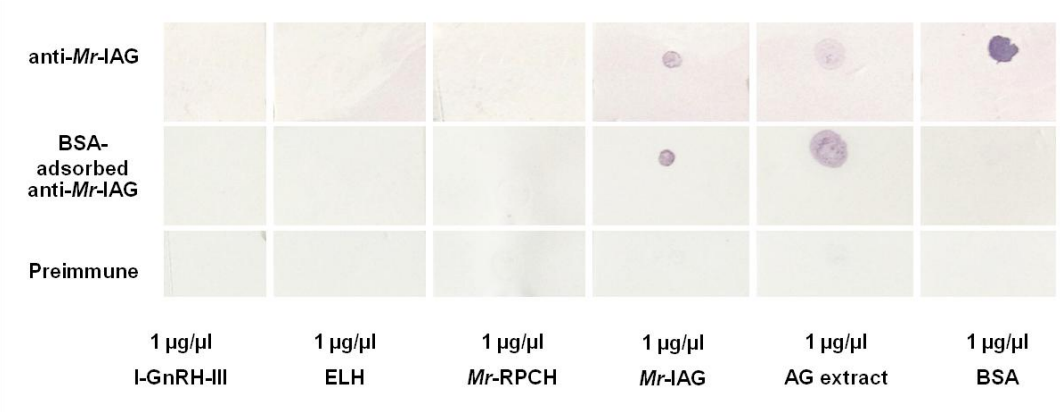

Figure 5.4 Dot-blot analysis showing specificity of anti-*Mr*IAG. From left to right: l-GnRH-III, ELH (egg-laying hormone), RPCH (red pigment concentrating hormone), *Mr*IAG peptide, AG crude extract, and BSA. Upper row: non-preadsorbed antibody, diluted 1:400 in PBS, used as a probe shows three positive dots of *Mr*IAG peptide, AG extract, and BSA; Middle row: Antibody (pre-adsorbed with 20% BSA and diluted 1:400 in PBS) used as a probe shows two positive dots of *Mr*IAG peptide and AG extract; and Lower row: Negative control using pre-immune serum shows that all dots are negative.

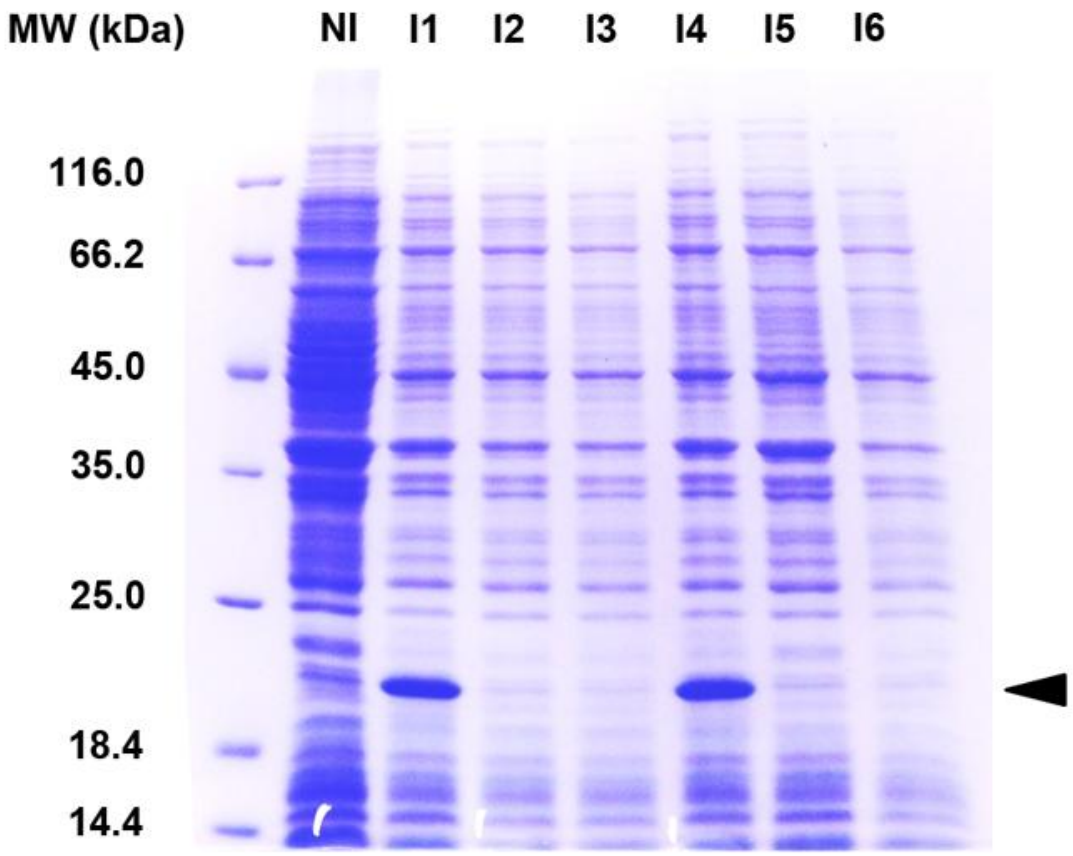

Figure 5.5 SDS-PAGE of recombinant *Mr*IAG (*rMr*IAG) in bacterial cell lysates 3 h after being induced by IPTG at 37ºC.

Lane 1: Protein marker

Lane 2: Non-induced clone

Lane 3-8: Induced clone 1-6

*rMr*IAG protein was shown in I1 and I4 at MW 20 kDa (black arrowhead).

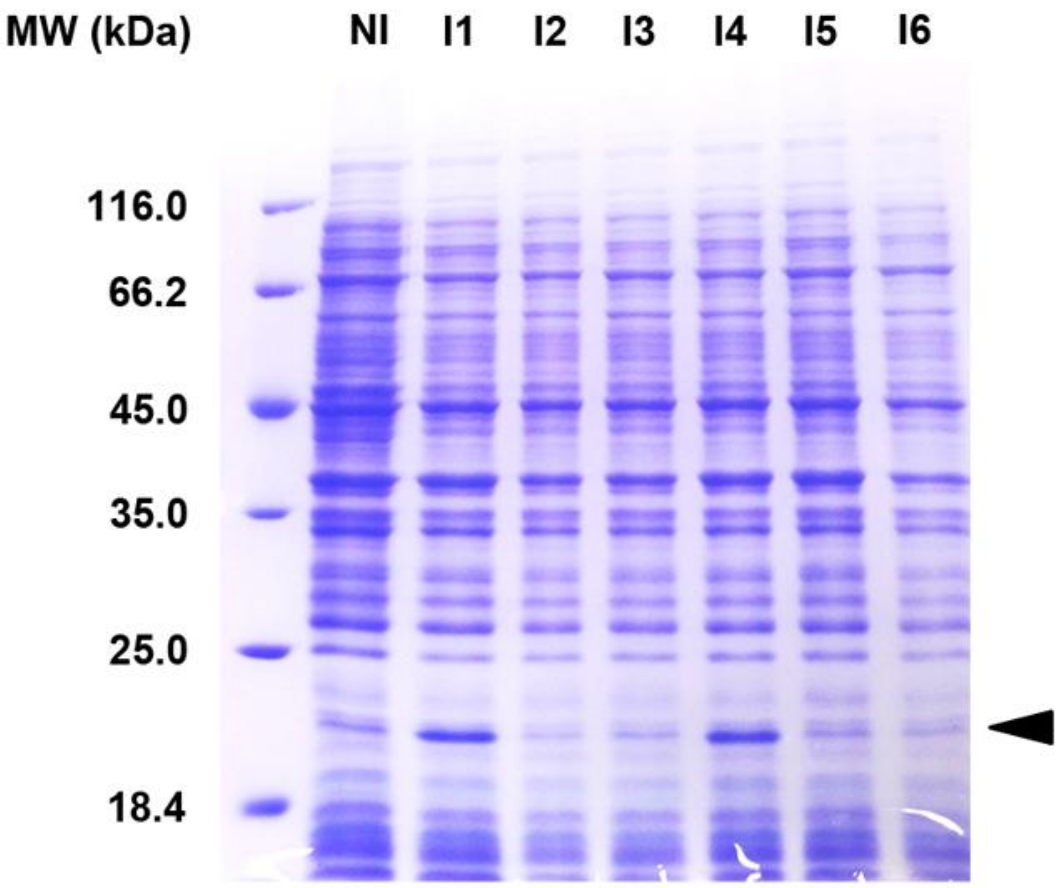

Figure 5.6 SDS-PAGE of recombinant *Mr*IAG (*rMr*IAG) in the bacterial cell lysates 3 h after being induced by IPTG at 25ºC.

Lane 1: Protein marker

Lane 2: Non-induced clone

Lane 3-8: Induced clone 1-6

*rMr*IAG protein was shown in I1 and I4 at MW 20 kDa (black arrowhead).

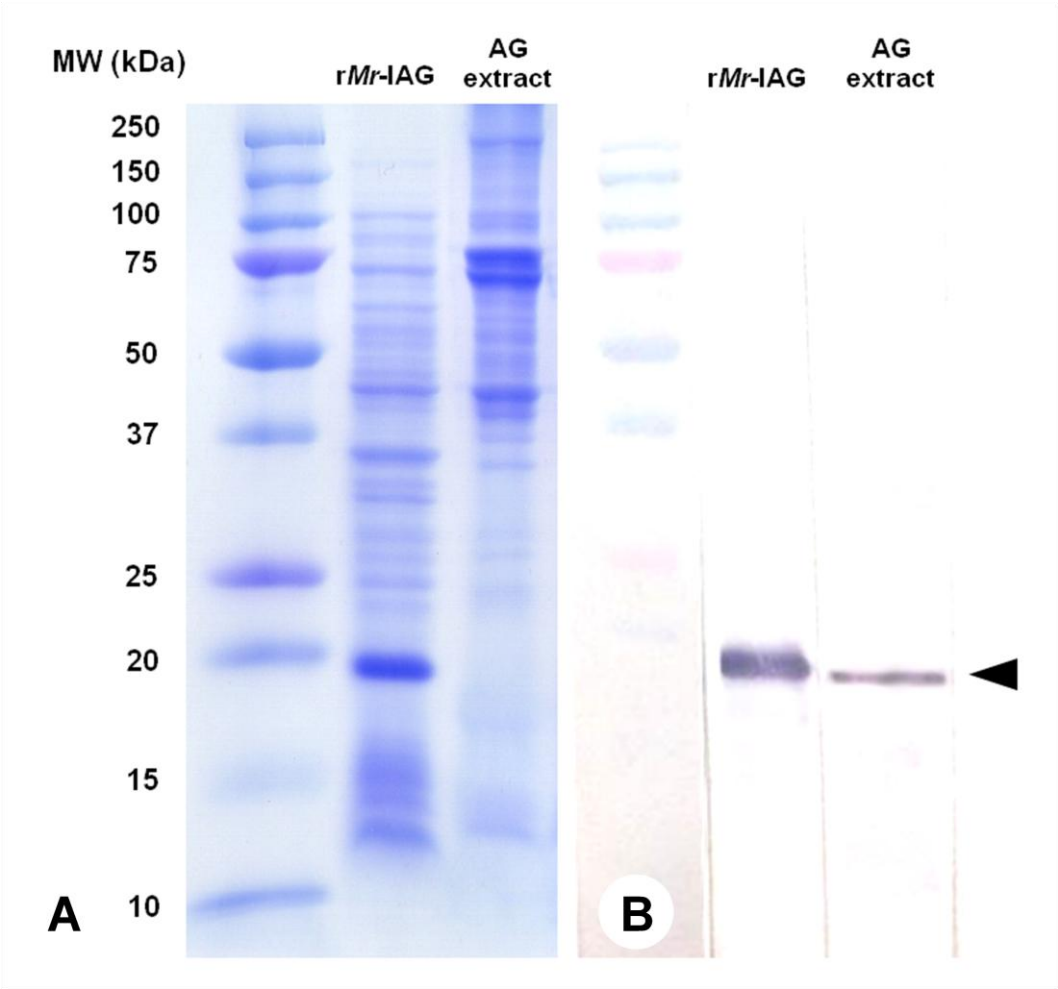

Figure 5.7 SDS-PAGE (A) and Western blot analysis (B) of *Mr*IAG in AG extract. (A) From left to right: Standard protein markers with molecular weights (MW) indicated at the left; recombinant *Mr*IAG (*rMr*IAG) in a bacterial cell lysate 3 h after being induced by IPTG; and the AG extract. (B) From left to right: Pre-stained standard proteins; inmmunodetection of *rMr*IAG in a bacterial cell lysate 3 h after being induced by IPTG; and inmmunodetection of *Mr*IAG in the AG extract, using BSA-adsorbed rabbit anti-*Mr*IAG (diluted 1:2000 in 0.1 M PBS) with 10 µg protein per lane. Arrowhead indicates the *rMr*IAG protein and *Mr*IAG protein in the AG extract at MW 17.6 kDa.

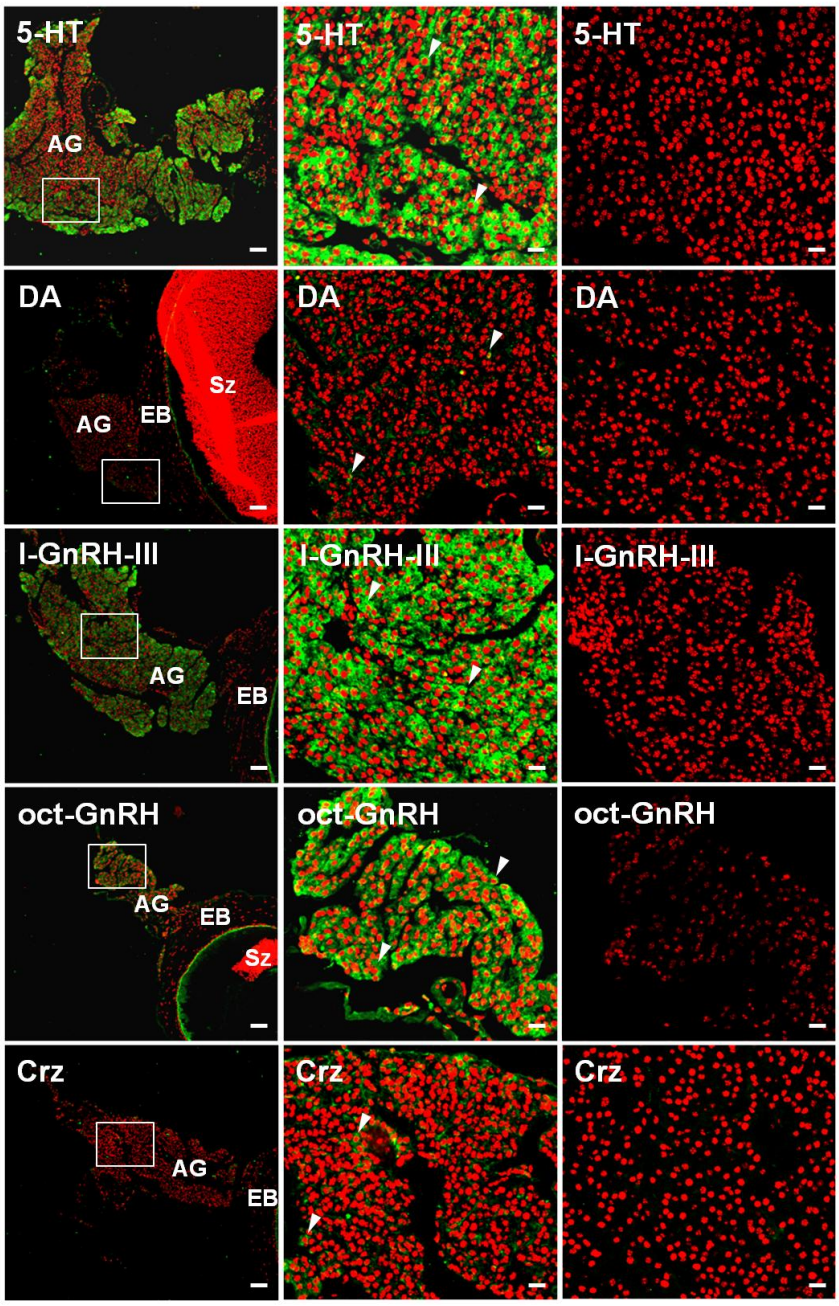

Figure 5.8 Immunoreactivity of insulin-like hormone (*Mr*IAG) in AG sections at day 12 by immunofluorescence assay, showing *Mr*IAG-*ir* (Green) and ToPro-3 (Red) nuclear staining. Low power micrographs (left column); high power micrographs of boxed areas (middle column); high power micrographs from the control group (right column) showing negative control AG, androgenic gland; EB, ejaculatory bulb; Sz, spermatozoa. Scale bars: left column = 100 µm; middle and right left columns = 25 µm.

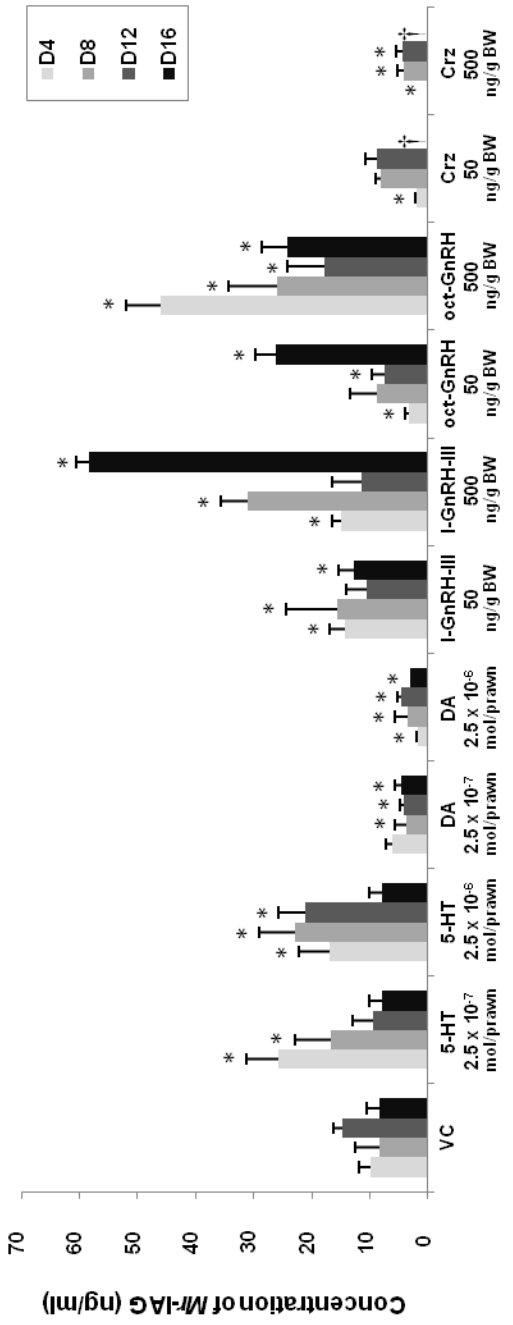

Figure 5.9 *Mr*IAG concentrations showing the calculated amounts of *M. rosenbergii* insulin-like hormone (*Mr*IAG) in the extracts of AGs, in each group at all doses. *Mr*IAG concentration in the histograms are shown as mean ± S.E. of duplicate samples at day 4, 8, 12, and 16, respectively; *, significant difference to VC ($P<0.05$); †, prawns died before day 16.

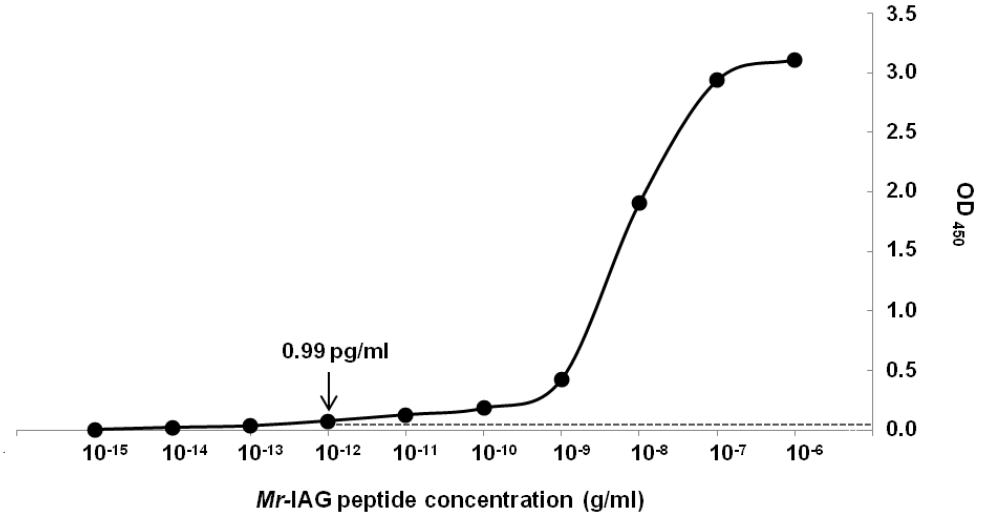

Figure 5.10 ELISA standard curve using a *Mr*IAG synthetic peptide (diluted 10^{-6} to 10^{-15}) detected with rabbit anti-*Mr*IAG (diluted 1:500 in 0.1 M PBS). The limit of detection was 0.99 pg/ml. The horizontal dashed line represents a base line calculated from the mean of negative controls plus 3 S.D. (Figure S4). The range of the standard curve corresponds with the range of experimental *Mr*IAG values (OD 0.2-3.0) in the ELISA of the control group AG extract and those of groups treated with neurotransmitters or neurohormones (Figure 5.9).

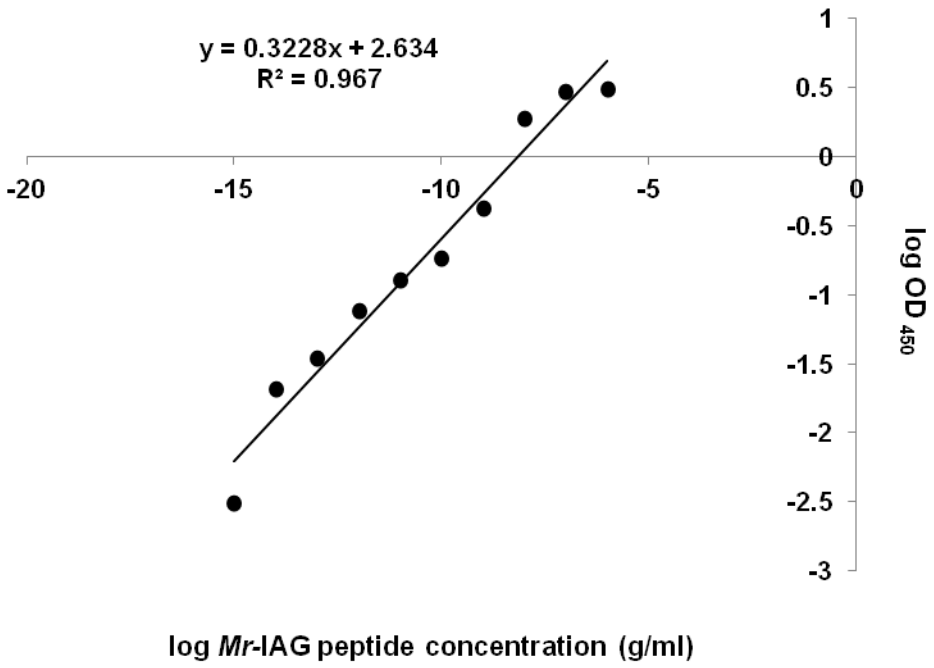

Figure 5.11 ELISA standard curve using a *Mr*IAG synthetic peptide (diluted 10^{-6} to 10^{-15}) detected with rabbit anti-*Mr*IAG (diluted 1:500 in 0.1 M PBS). The relationship of log OD and log concentration was represented by the equation $y = 0.3228x + 2.634$, $R^2 = 0.967$.

5.2 Temporal expressions of *MrIAG* in larvae and postlarvae, and the use this gene as a marker for selecting male offsprings

5.2.1 Performance of postlarvae culture

The survival trend of PL1 during experiments was highest in PL1D7 at 95.6 %, followed by PL1D6 at 93.8 and PL1D5 93.0 %, whereas PL1D2 showed only 73.8 % survival (Figure 5.12). From our observation, the mortality of prawns usually occurred through by cannibalism especially in the earlier stages. However, the survival trend of PL1 was generally over 70%, which showed that our culturing conditions were suitable for PL prawn.

5.2.2 Morphology of postlarvae

The PL prawns in crops PL1D1, PL1D3, PL1D5, PL1D7, PL1D9, PL1D11, and PL1D13 as view in darkfield mode of a stereo microscope showed similar external features (Figure 5.13A) but different only in the body length at low and higher magnification of head and body regions (Figure 5.13B), and tail regions of PL1D11 (Figure 5.13C).

5.2.3 Temporal expression of *MrIAG*

The results of RT-PCR revealed that *MrIAG* gene was expressed early even in larval (LV) stage even though the band was not intense (Figure 5.14 lane 2). Later in PL1D1-PL1D7 the *MrIAG* band with the length of 394 bp became progressively more intense until it reached the highest intensity in the fully mature AG (n = 15) (Figure 5.14). Therefore, the *MrIAG* gene can be used as a male marker in the early flipping prawns because its expression could be detected even at the first day of PL1.

5.2.4 *MrIAG* expression in a single prawn of each crop

In order to detect the IAG expression in each prawn (Figure 5.14), we selected PL1-4 at day 8 to ensure that the mass of AG in each prawn was large enough to detect the *MrIAG* expression. The results showed that all prawn in PL1D8 showed PCR product with 12 having high intensity and 3 having low intensity (n = 15). The

PL2D8 crop showed 5 PL prawns with high and 5 with low intensity (n = 15). In PL3D8 showed 5 PL prawns with high and 4 with low intensity (n = 15). In contrast, in PL4D8 crop we found only 1 PL prawns with high and 2 with low intensity (n = 5).

From this RT-PCR result, the percent of male prawn were calculated and shown in Figure 5.15 B. The PL1D8 or first crop of flipping prawn had 80% male with high and 20% male of low IAG expression. The second and third crops of flipping prawns (PL2D8 and PL3D8) had 33.33% male with high and 33.33% and 26.67% male with low expression of *IAG*. The forth crop of flipping prawns (PL4D8) had only 20% male with high and 40% male with low *IAG* expression.

5.2.5 The percent of male prawn in each flipping day quantified by gonopore complex

After maintaining PL1-PL3 prawns for 4 months, we estimated the proportion of young adult male prawns by observing the presence of male gonopore at the base of the fifth walking legs as shown in Figure 5.16. We found that percentage of male in PL1 was at 81.5% and PL2 at 76.1%, which were significantly different when compared with PL3 at 64.6% with $P < 0.05$ (Table 5.1; Fig. 5.17). It was unfortunate that most prawns in PL4 crop died before the end of the experiment with the percents of maturity in the former three crops (PL1, PL2, PL3) were 80.8, 72.1, 59.9 respectively.

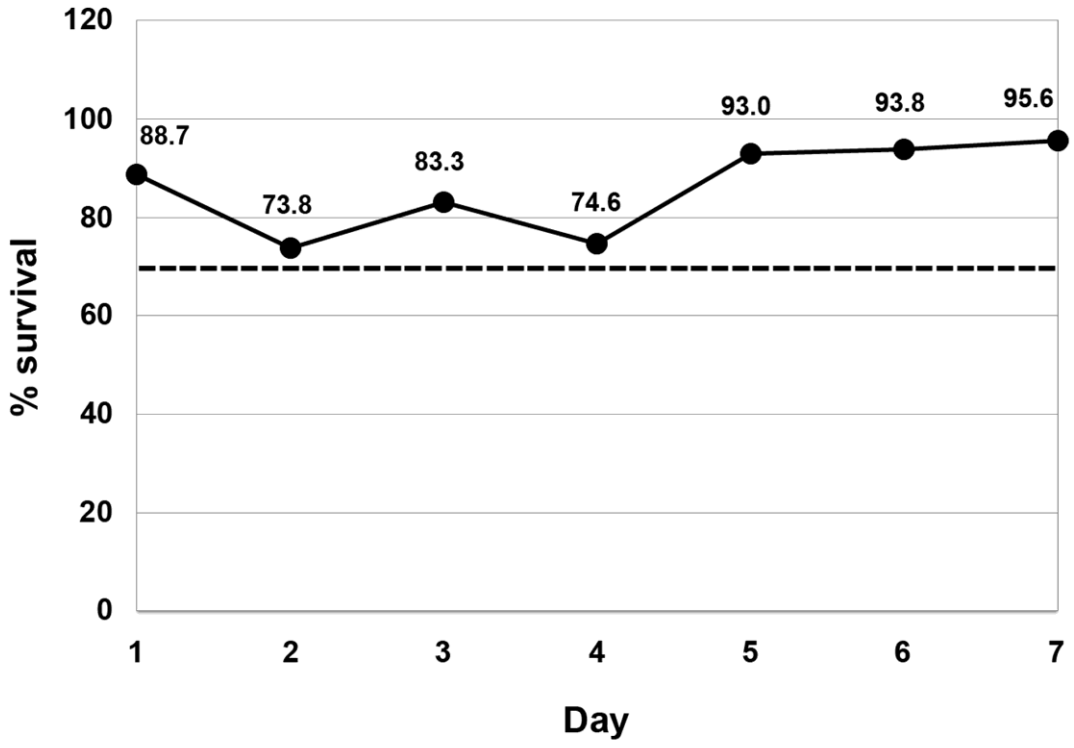

Figure 5.12 The survival of PL1 during the period of the experiments, which was over 70% (dash line) with the highest rate in PL1D7.

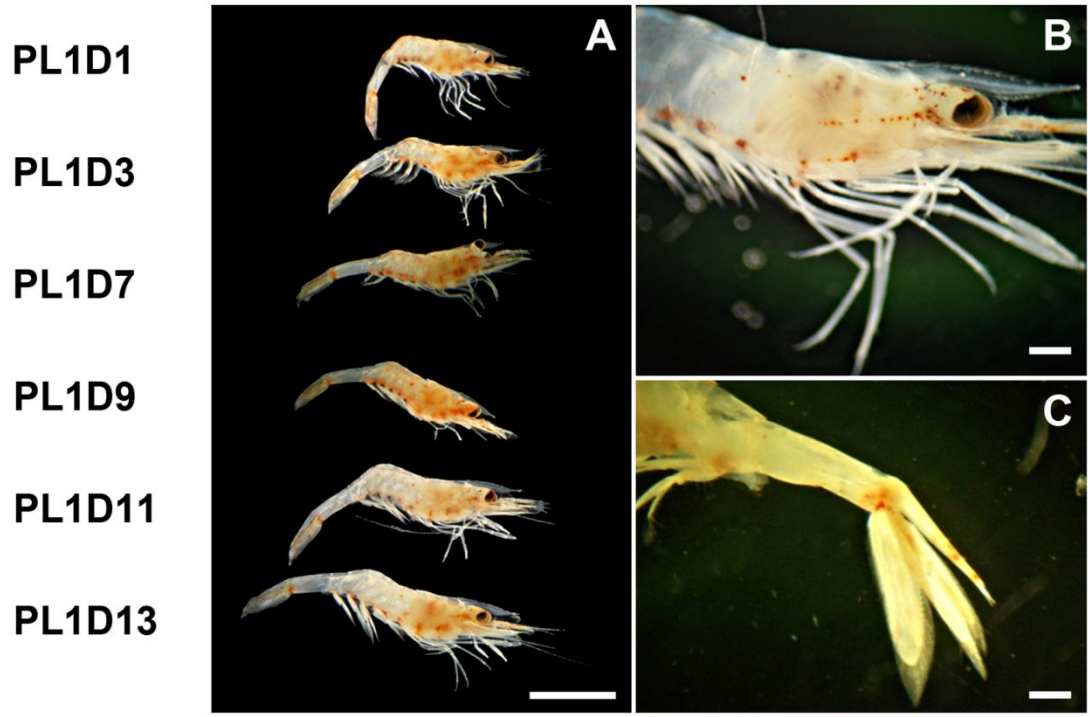

Figure 5.13 An external morphology of PL prawns showing (A) the size of PL1 prawns from day 1, 3, 5, 7, 9, 11, and 13. (B) A higher magnification of head and body regions of PL1D11. (C) A higher magnification of tail region of PL1D11 viewed in darkfield mode of the stereo microscope. Scale bar (A) = 5 mm; (B, C) = 2 mm

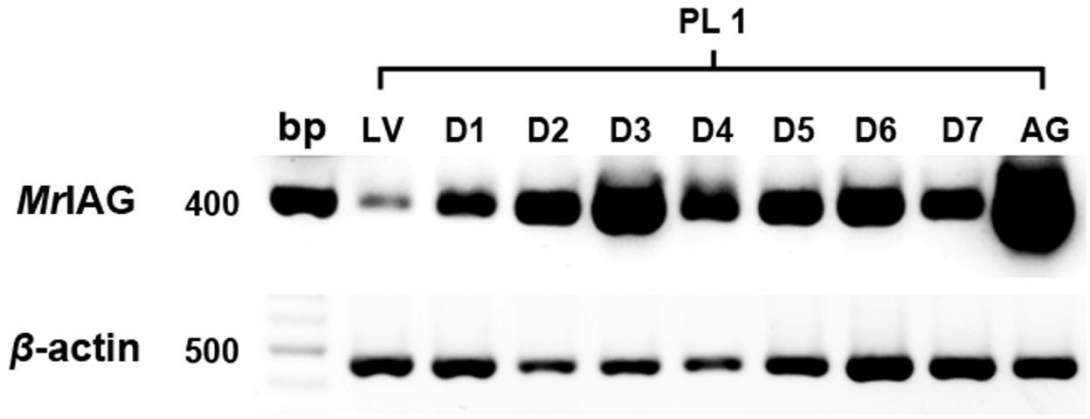

Figure 5.14 RT-PCR showing the expression of *Mr*IAG in PL prawns at 394 bp. The mRNA was extracted from LV, PL1 from days 1-7 (PL1D1-PL1D7), and the mRNA from the AG from fully mature (blue claw) males was check as a positive control (n = 15).

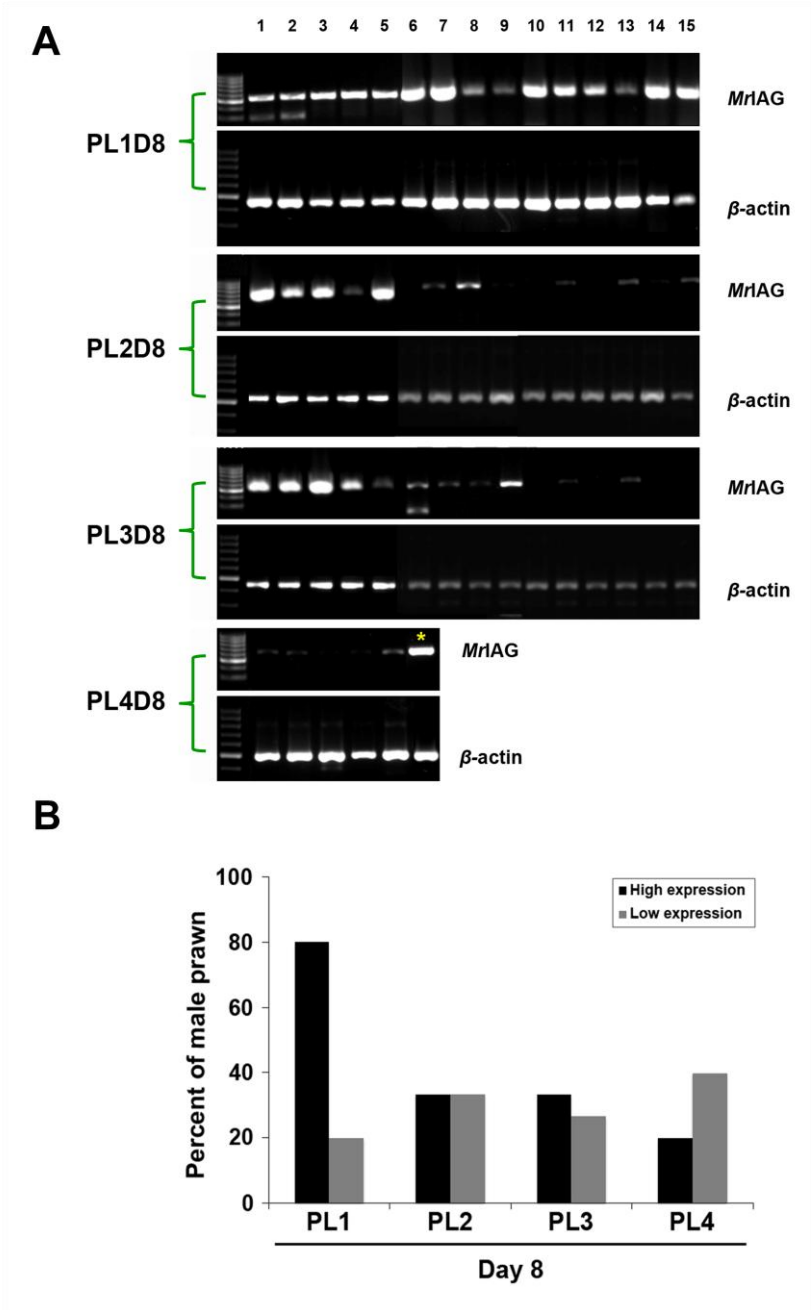

Figure 5.15 *Mr*IAG expressions in single prawn of each flipping day. (A) The mRNA was extracted from PL1-4 at day 8, and fully mature AG (*) as positive control. *Mr*IAG bands were mostly presented in PL1D8. (B) Percent of male prawn calculated by *Mr*IAG expression in each flipping day, including PL1-3 (n = 15) and PL4 (n = 5). The PL1D8 or first group of flipping prawn have 80% male of high and 20% male of low expression band.

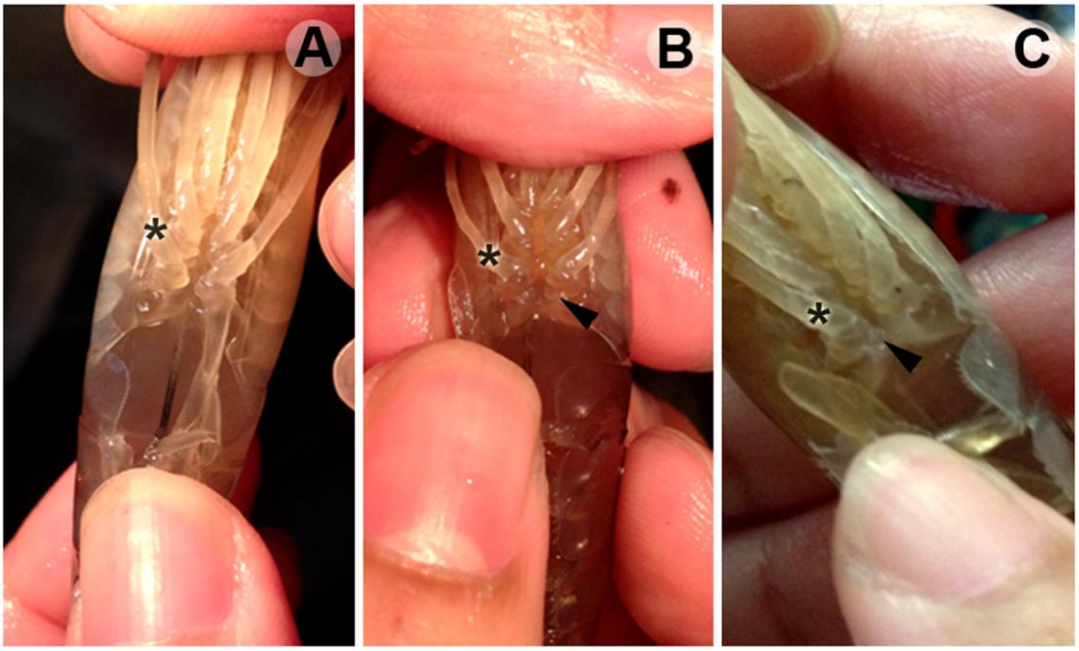

Figure 5.16 The ventral aspect of prawns in PL1D1 showing (A) the gonopore is absents in female at the base of the third walking leg, (B-C) the opening of gonopores (black arrowhead) is presented at the base of the fifth periopods (*) in male. Scale bar (A) = 5 mm; (B, C) = 2 mm

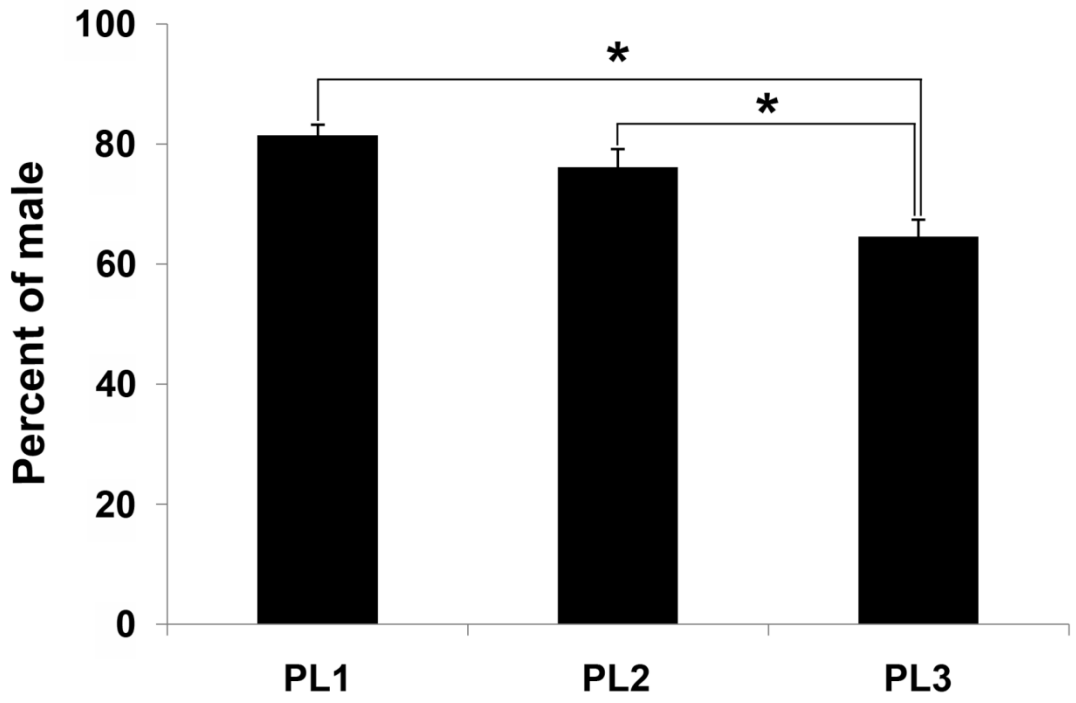

Figure 5.17 Percents of male prawns in the PL1, PL2, Pl3, crops that had been cultured for 120 days, at which time male could be identified by the presence of male gonopore at the base of the fifth walking legs (mean ± SD). The males in PL1 is at 81.5%, PL2 at 76.1%, which when compared with PL3 (at 64.6%), was significantly different at $P < 0.05$.

Table 5.1 The numbers and percent ages of male prawns counted by observing the presence of the male gonopore on each flipping day (mean ± SD).

PL	Lot	Male	Female	Total	Percent of Male	Mean ± SD
1	1	81	20	101	80.2	81.5 ± 1.8 *
	2	72	15	87	82.8	
2	1	37	13	50	74.0	76.1 ± 3.0 *
	2	18	5	23	78.3	
3	1	4	2	6	66.7	64.6 ± 2.9
	2	10	6	16	62.5	

* = significantly at $P < 0.05$

5.3 Changes of phosphatidylcholine and fatty acids in germ cells during testicular maturation in three developmental male morphotypes of *M. rosenbergii* revealed by imaging mass spectrometry

5.3.1 Histology of the seminiferous tubules

Spermatogenesis within the STs has been classified into 9 stages corresponding to the presence of different types of spermatocytes, spermatids, and spermatozoa (Poljaroen et al., 2011). In our research using 10 µm-thick cryosection, it was difficult to clearly identify all 9 stages of the STs. However, based on the histological outlines and abundance of spermatogonia (Sg), spermatocytes (Sc), spermatids (St), and spermatozoa (Sz) present in the tubules we could identify the stages of the STs and separated them into three groups representing early, middle, and late stages of spermatogenesis (Figure 5.18 a-e, f-j ,k-o). Group A (including stages I-V), contained Sg and nurse cells (Nc) that were located on the basement membrane, and mostly Sc (Figure 5.18 a-e). Group B (including stages VI-VIII), contained some Sg and Sc, but mostly St and immature Sz with condensed chromatin (Figure 5.18 f-j). Group C (stage IX), contained mostly mature Sz with de-condensed chromatin (Figure 5.18 k-o). In all stages, the STs were surrounded by intertubular area (IT) made up mainly of connective tissues. All three groups of ST stages were found in the three male morphotypes, but in different proportions. For example, SM contained mostly group A, OC contained mostly group B, and BC contained mostly group C.

5.3.2 Quantification of lipids by thin layer chromatography

The extracted lipids were separated by TLC, and the highest intensity signals were found in PC bands of each group. The PCs bands were expressed as mean ± S.D. which showed different amounts in each of the ST groups (Figure 5.19 2A) and the male developmental morphotypes (Figure 5.19 2B). The STs of group B which contained mostly spermatids and some immature sperms showed significantly higher intensities compared with group A and C ($P<0.05$) (Figure 5.19). The highest amounts of PCs could be observed in the OC males, which is the transitional stage from SM to

BC male, and the lowest PC amounts were observed in BC males (with significant difference at $P<0.05$) (Figure 5.19 2B).

5.3.3 Identification of lipids by tandem mass spectrometry (MS/MS)

MS profile showed all ions detected in STs of OC (Figure 5.20). MS/MS analysis showed product ions from precursor ions at *m/z* 780.5 (Figure 5.21 A), and *m/z* 798.5 (Figure 5.21 B). These signals were identified as [PC (16:0/18:2) + Na]$^+$ and [PC (16:0/18:1) + K]$^+$, respectively. The product ions from the precursor ion at *m/z* 780.5 represented neutral losses of a PC head group [$(CH_3)_3N(CH_2)_2PO_4H$] at *m/z* 597.5 and trimethylamine [$(CH_3)_3N$] at *m/z* 721.5. These neutral losses are common for PCs. Another peak at *m/z* 575.5 indicates the replacement of adduct ion from Na^+ to H^+. The minor peaks at *m/z* 465.3 and 441.3 correspond to neutral losses of FAs (16:0 and 18:2) from a peak at *m/z* 721.5. Therefore, these molecules were assigned as [PC (16:0/18:2) + Na]$^+$ (Figure 5.21 A). The product ions from the precursor ion at *m/z* 798.5 represents neutral losses of a PC head group [$(CH_2)_2PO_4H$] at *m/z* 615.5 and trimethylamine [$(CH_3)_3N$] at *m/z* 739.5. The peak at *m/z* 577.5 indicates the replacement of adduct ion from K^+ to H^+. The minor peaks at *m/z* 483.5 and 457.5 correspond to neutral losses of FAs (16:0 and 18:1) from a peak at *m/z* 739.5. Therefore, these molecules were assigned as [PC (16:0/18:1) + K]$^+$ (Figure 5.21 B).

All signals from ion images (Table 5.2) were identified in the same way as the two signals described above, and comprised of *m/z* 756.5 [PC (16:0/16:1) + Na]$^+$, 760.5 [PC (16:0/18:1) + H]$^+$, 782.5 [PC (16:0/18:1) + Na]$^+$, 798.5 [PC (16:0/18:1) + K]$^+$, 780.5 [PC (16:0/18:2) + Na]$^+$, 796.5 [PC (16:0/18:2) + K]$^+$, 784.5 [PC (16:0/18:0) + Na]$^+$, 800.5 [PC (16:0/18:0) + K]$^+$, 804.5 [PC (18:2/18:2) + Na]$^+$, 806.5 [PC (18:1/18:2) + Na]$^+$, 808.5 [PC (18:0/18:2) + Na]$^+$, 824.5 [PC (18:0/18:2) + K]$^+$, and 810.5 [PC (18:0/18:1) + Na]$^+$. The signals that represented omega-3 FAs (Table 5.3) were 826.5 [PC (18:2/20:5 (EPA)) + Na]$^+$, 846.5 [PC (18:0/20:5 (EPA)) + K]$^+$, 828.5 [PC (16:0/22:6 (DHA)) + Na]$^+$, 844.5 [PC (16:0/22:6 (DHA)) + K]$^+$, 870.5 [PC (18:1/22:6 (DHA)) + K]$^+$, and 872.5 [PC (18:0/22:6 (DHA)) + K]$^+$, and the signals that represented omega-6 were 820.5 [PC (16:0/20:4 (ARA)) + K]$^+$, 830.5 [PC (18:1/20:4 (ARA)) + Na]$^+$, and 832.5 [PC (18:0/20:4 (ARA)) + Na]$^+$.

5.3.4 Distributions of lipids by imaging mass spectrometry (IMS)

Ion images indicating high intensity of PCs related with the area in Figure 5.22, including *m/z* 798.5 [PC (16:0/18:1) + K]$^+$, 808.5 [PC (18:0/18:2) + Na]$^+$, 826.5 [PC (18:2/20:5 (EPA)) + Na]$^+$, and 872.5 [PC (18:0/22:6 (DHA)) + K]$^+$ in Figures 5.23 and 5.25, and *m/z* 756.5 [PC (16:0/16:1) + Na]$^+$, 780.5 [PC (16:0/18:2) + Na]$^+$, 800.5 [PC (16:0/18:0) + K]$^+$, 804.5 [PC (18:2/18:2) + Na]$^+$, 806.5 [PC (18:1/18:2) + Na]$^+$, 810.5 [PC (18:0/18:1) + Na]$^+$, 820.5 [PC (16:0/20:4 (ARA)) + K]$^+$, 830.5 [PC (18:1/20:4 (ARA)) + Na]$^+$, 832.5 [PC (18:0/20:4 (ARA)) + Na]$^+$, 844.5 [PC (16:0/22:6 (DHA)) + K]$^+$, 846.5 [PC (18:0/20:5 (EPA)) + K]$^+$, and 870.5 [PC (18:1/22:6 (DHA)) + K]$^+$ in Figure 5.24, showed the distributions pattern of PCs in each ST group of OC males, particularly in groups A and B, and the IT (Tables 5.2 and 5.3). The H&E-stained sections of the same areas confirmed that the identifications of the ST groups were correct (Figure 5.22).

The distribution of PCs were divided into 4 distinct patterns: (i) the PCs presented in all groups of STs comprised of PC (16:0/18:1) represented by *m/z* 760.5, 782.5, and 798.5 (Figure 5.23 d-f and 5.25 d-f; Table 5.2), PC (16:0/18:2) represented by *m/z* 780.5 and 796.5 (Figure 5.24 b; Table 5.2), PC (18:2/18:2) represented by *m/z* 804.5 (Figure 5.24 d; Table 5.2), and PC (18:1/20:4 (ARA)) represented by *m/z* 830.5 (Figure 5.24 h; Table 5.3),which showed high signal intensities in developing germ cells area containing Sg, Sc, and St and the IT. The signal corresponding to *m/z* 798.5 showed the highest intensity in every group of STs (Figure 5.23 d-f and 5.25 d-f; Table 5.2). However, we did find areas containing late St and Sz in groups B and C that showed very low intensity of *m/z* 798.5 (Figure 5.25 e-f). (ii) The PCs presented in the STs of groups A and B, comprised of PC (16:0/18:0) represented by *m/z* 784.5 and 800.5 (Figure 5.24 c; Table 5.2), PC (16:0/20:4 (ARA)) represented by *m/z* 820.5 (Figure 5.24 g; Table 5.3), PC (18:2/20:5 (EPA)) represented by *m/z* 826.5 (Figure 5.23 j-l and 5.25 j-l; Table 5.3), PC (18:0/20:5 (EPA)) represented by *m/z* 846.5 (Figure 5.24 k; Table 2), and PC (18:0/18:2) represented by *m/z* 808.5 and 824.5 (Figure 5.23 g-i and 5.25 g-i; Table 5.2), showed the highest signal intensities in developing germ cell areas and the IT. (iii) The PCs presented in the STs of groups B and C, comprised of PC (16:0/16:1) represented by *m/z* 756.5 (Figure 5.24 a; Table 5.2), PC (18:1/18:2) represented by *m/z* 806.5 (Figure 5.24 e; Table 5.2), and PC

(18:0/18:1) represented by *m/z* 810.5 (Figure 5.24 f; Table 5.2), also showed high signal intensities in the IT. (iv) Lastly, the PCs presented only in the STs of group A, comprised of PC (16:0/22:6 (DHA)) represented by *m/z* 828.5 and 844.5 (Figure 5.24 j; Table 5.3), PC (18:0/20:4 (ARA)) represented by *m/z* 832.5 (Figure 5.24 i; Table 5.3), PC (18:1/22:6 (DHA)) represented by *m/z* 870.5 (Figure 5.24 l; Table 5.3), and [PC (18:0/22:6 (DHA)) represented by *m/z* 872.5 (Figure 5.23 m-o and 5.25 m-o; Table 5.3), showed high signal intensities in developing germ cell areas.

5.3.5 Quantification of fatty acids by gas chromatography-mass spectrometry (GC-MS)

FAs in lipid extractions from the testes of each developmental male morphotype were quantified using GC-MS, and it was found that the FAs which were detected in the testes of the three morphotypes consisted of 14:0, 15:0, 16:0, 17:0, 18:0, 16:1, 18:1, 18:2, 20:1, 20:2, 20:4, 20:5, and 22:6. In term of relative quantities it was shown that during the development from SM to mature BC, the OC testes contained highest amounts of FAs 16:0, 18:0, 16:1, 18:1, 18:2, 20:1 (with significant difference at $P<0.05$), and contained higher amounts of 14:0, 15:0, 20:2 when compared with BC (with significant difference at $P<0.05$) while the differences were not significant when compared to SM (Figure 5.26 A). Moreover, testes of SM and OC contained higher amounts of FAs 17:0, and 20:5 (EPA) when compared to BC (with significant difference at $P<0.05$), whereas FAs 20:4 (ARA) and 22:6 (DHA) showed no statistical difference among the testes of the three groups (Figure 5.26 A). However, FA ratios showed that the testes of SM contained higher accumulations of 17:0, 20:1, 20:2, 20:5 (EPA) and 22:6 (DHA) when compared with OC (with significant difference at $P<0.05$) while there were no significant differences between SM and BC (Figure 5.26 B).

In the same way, it was shown that during the development from STs of group A to C of OC testes, STs of group B showed higher amount of 15:0, 16:0, 17:0, 18:0, 18:1, 18:2, 20:2, and 20:5 when compared with BC (with significant difference at $P<0.05$) (Figure 5.27).

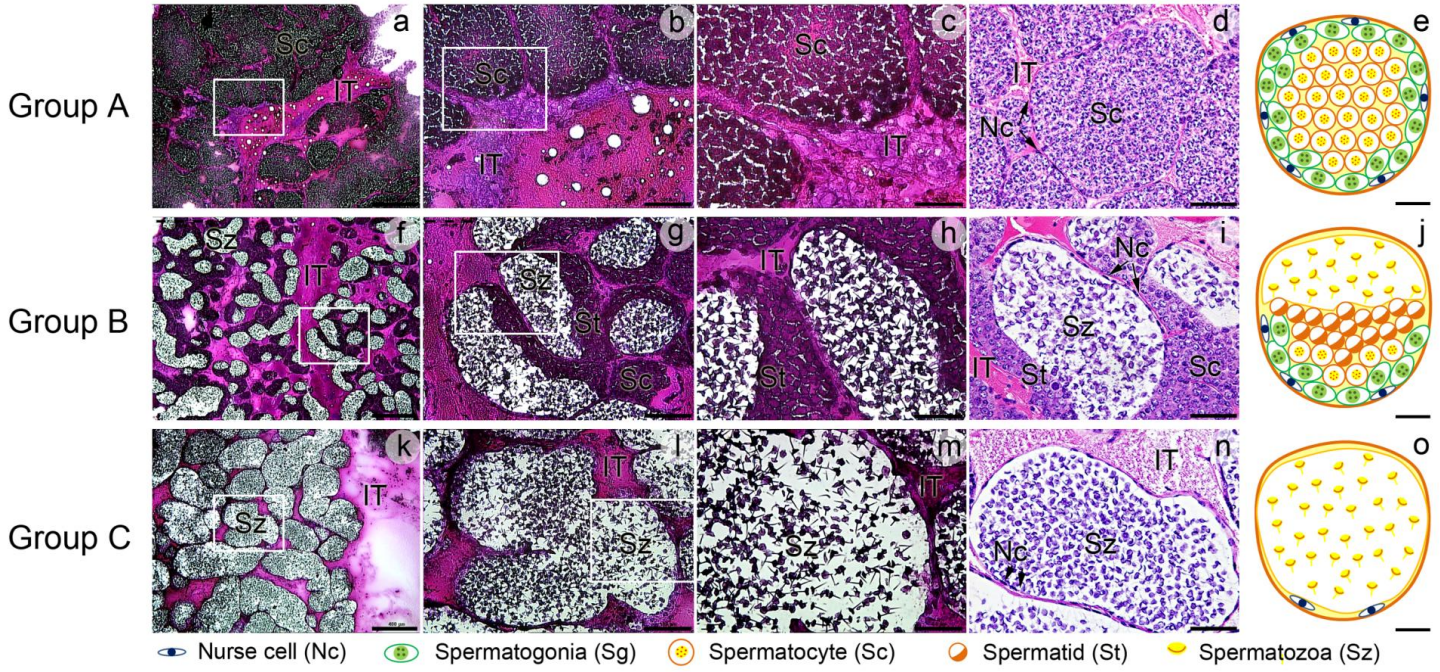

Figure 5.18 Micrographs of cryosections (a-c, f-h, k-m), H&E-stained paraffin sections (d, i, n), and illustrations of the three groups of seminiferous tubules (STs) in OC males (e, j, o).–Group A STs (a-e) contain mostly spermatogonia (Sg) and nurse cells (Nc) close to the basement membrane, and few spermatocytes (Sc) in the lumen. Group B STs (f-j) contain Sg, Nc, numerous spermatids (St), and immature spermatozoa (Sz) within a lightly stained lumen. Group C STs (k-o) contain mostly fully mature Sz (with decondensed chromatin) and Nc close to the basement membrane. All stages of the STs are surrounded by intertubular areas (IT). Scale bars: a, f, k = 400 μm; b, g, l = 100 μm; c-d, h-i, m-n = 50 μm; e, j, o = 20 μm.

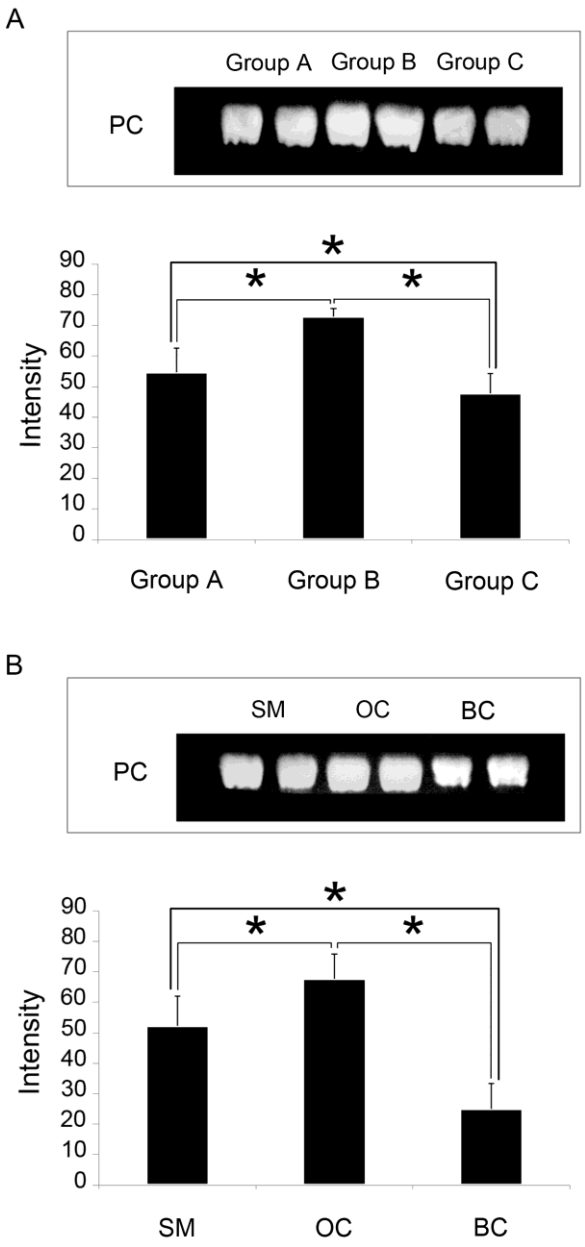

Figure 5.19 Separation and identification of phosphatidylcholines (PCs) by thin-layer chromatography (TLC) showing duplicated bands (upper panels) and histograms of the intensity of PCs (lower panel) in (A) each group of seminiferous tubules (ST), and (B) testes of the three developmental male morphotypesSM = small male; OC = orange claw male; BC = blue claw male. Bar = S.D.; * = significant difference at $P<0.05$.

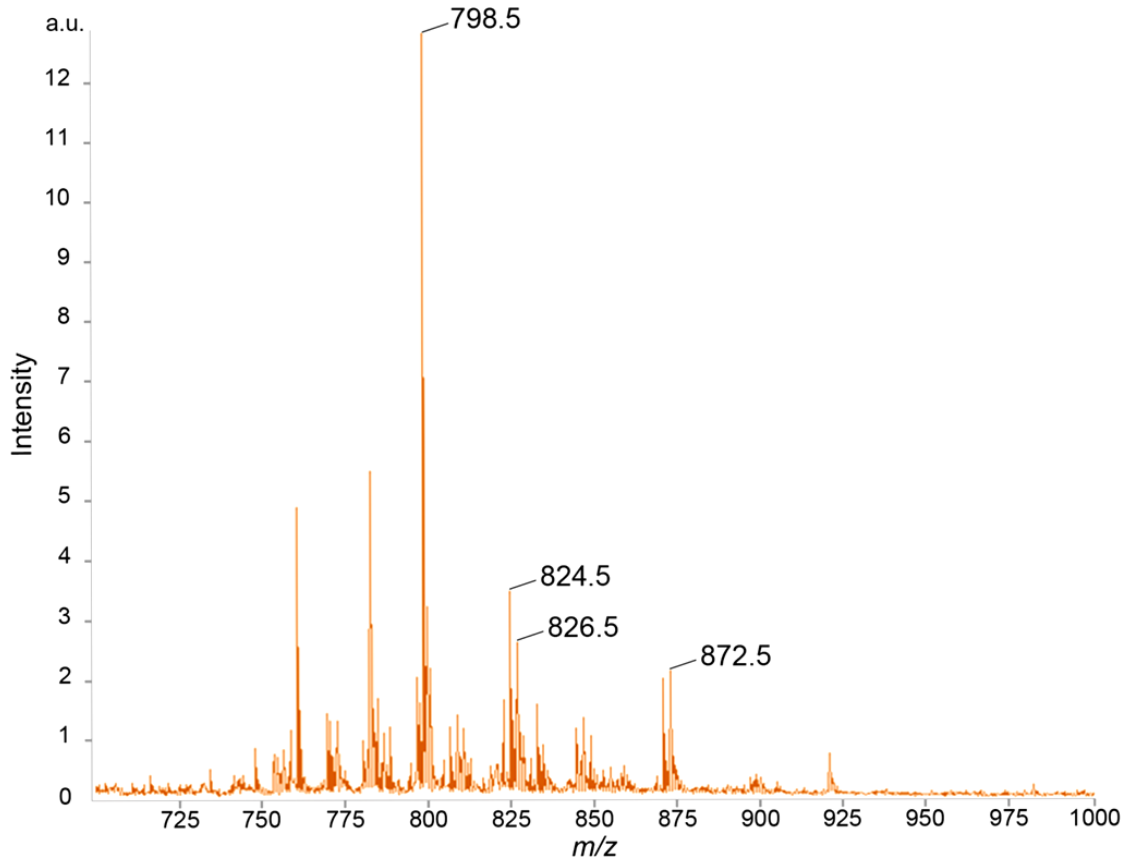

Figure 5.20 MS analysis showing all spectra detected in the STs of OC.

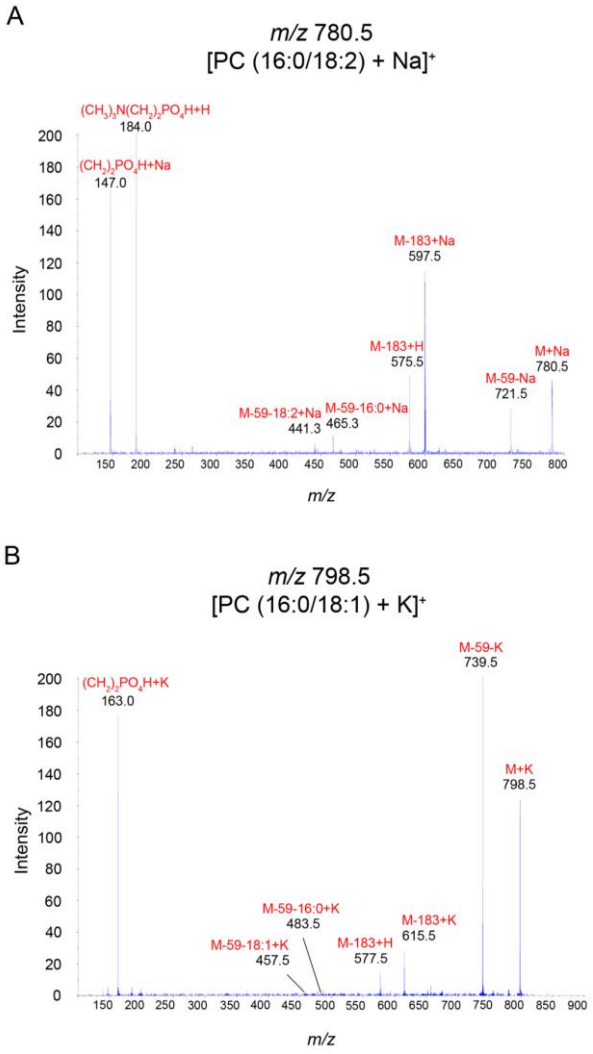

Figure 5.21 MS/MS analysis showing product ions from the precursor ions at (A) *m/z* 780.5 and (B) *m/z* 798.5. The product ions from the precursor ion at *m/z* 780.5 represent neutral losses of a PC head group $[(CH_3)_3N(CH_2)_2PO_4H]$ at *m/z* 597.5 and trimethylamine $[(CH_3)_3N]$ at *m/z* 721.5. The minor peaks at *m/z* 465.3 and 441.3 correspond to neutral losses of FAs (16:0 and 18:2) from a peak at *m/z* 721.5. Therefore, the molecule was assigned as [PC (16:0/18:2) + Na]$^+$. The product ions from the precursor ion at *m/z* 798.5 represent neutral losses of the PC head group $[(CH_2)_2PO_4H]$ at *m/z* 615.5 and trimethylamine $[(CH_3)_3N]$ at *m/z* 739.5. The minor peaks at *m/z* 483.5 and 457.5 correspond to neutral losses of FAs (16:0 and 18:1) from a peak at *m/z* 739.5. Therefore, the molecule was assigned as [PC (16:0/18:1) + K]$^+$.

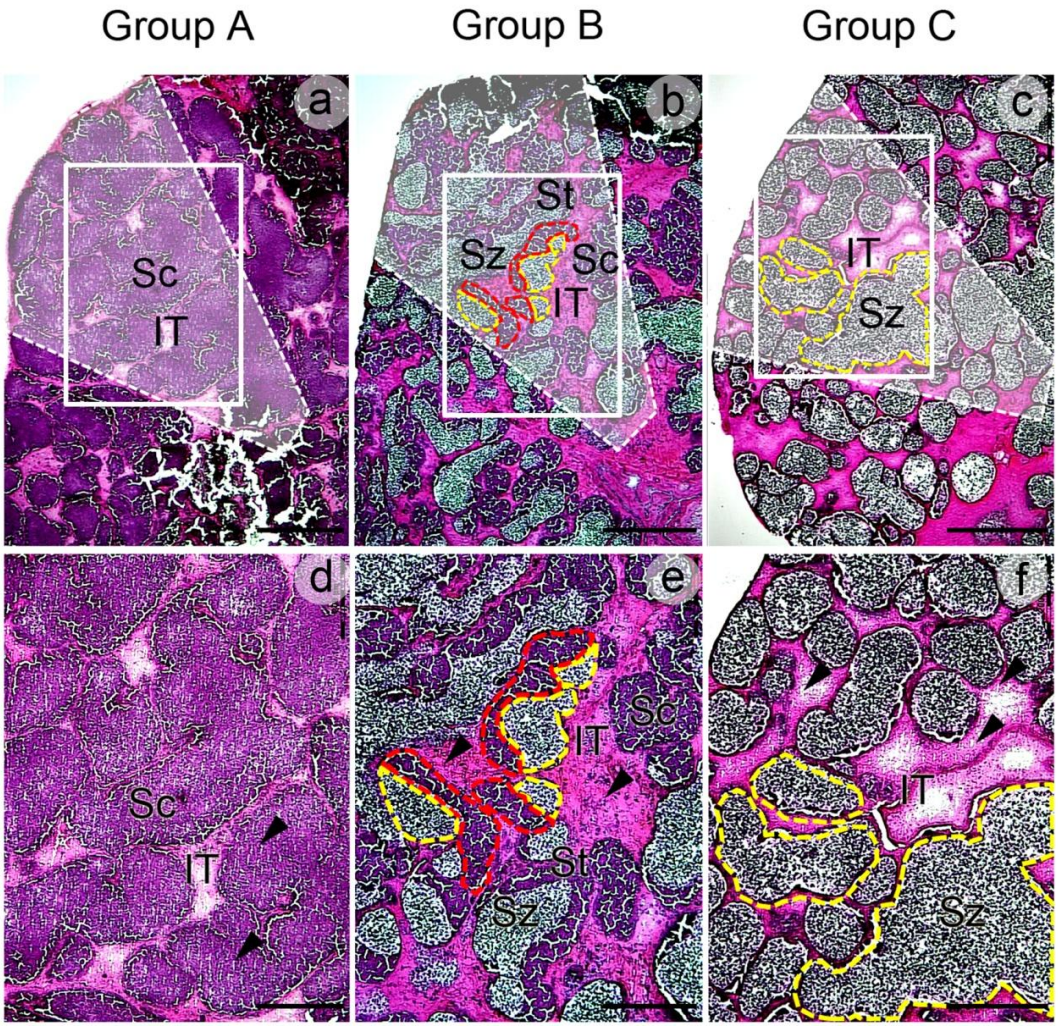

Figure 5.22 Micrograph from H&E-stained sections showing the areas in the three ST groups being analysed in Figure 5.23. The upper row (a, b, c) shows low magnification and the lower row (d, e, f) shows higher magnifications of the boxed areas. Each of the group B STs contains a narrow crescentric strip of early germ cells surrounded by red dashed lines, while the remaining part of the tubule contains spermatozoa surrounded by yellow dashed lines (b, e). In contrast, all group C STs contain only spermatozoa (surrounded by yellow dashed line) with no developing cell areas (c, f). These areas were analysed by IMS. The arrowheads indicate the laser scars that appear after IMS analyses. Sc = spermatocytes; Sz = spermatozoa; St = spermatids; IT = intertubular Scale bars; upper layer = 400 μm, lower layer = 200 μm.

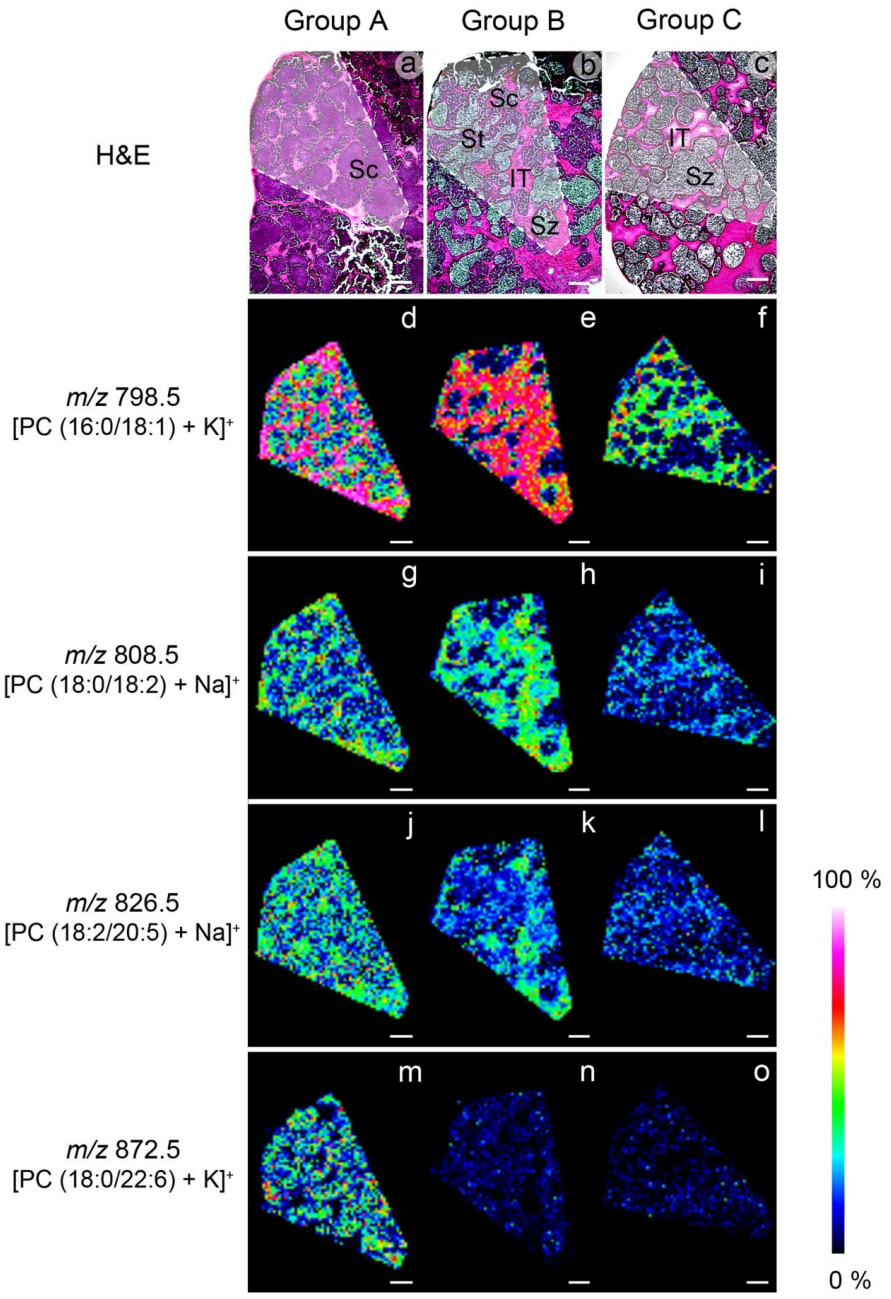

Figure 5.23 IMS showing different intensities and distributions of PCs in each group of seminiferous tubules in cryosections of the OC males (d-o), compared with picture of the same sections stained with H&E (a-c). Sc = spermatocytes; Sz = spermatozoa; St = spermatids; IT = intertubular area; Scale bars = 200 μm; Relative intensity bar shows the intensity level of the ion images.

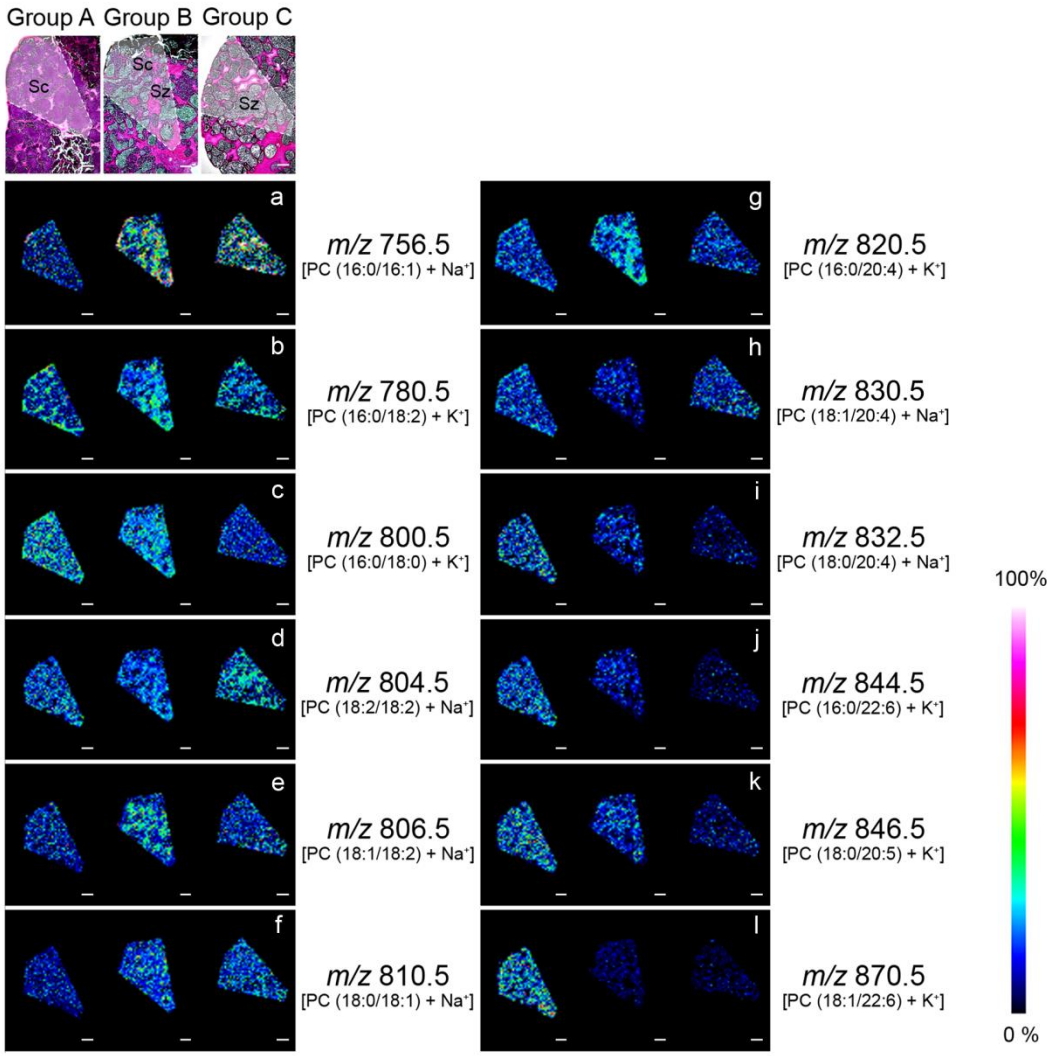

Figure 5.24 Ion images show different intensities and distributions of PCs in each seminiferous group in cryosections of the OC testes, compared with H&E staining of the same areas (Top row). The signals also appear to be mainly in early germ cells and intertubular area (IT) of the three groups of STs. Sz = spermatozoa; Scale bars = 200 μm; Relative intensity bar shows the intensity level of ion images.

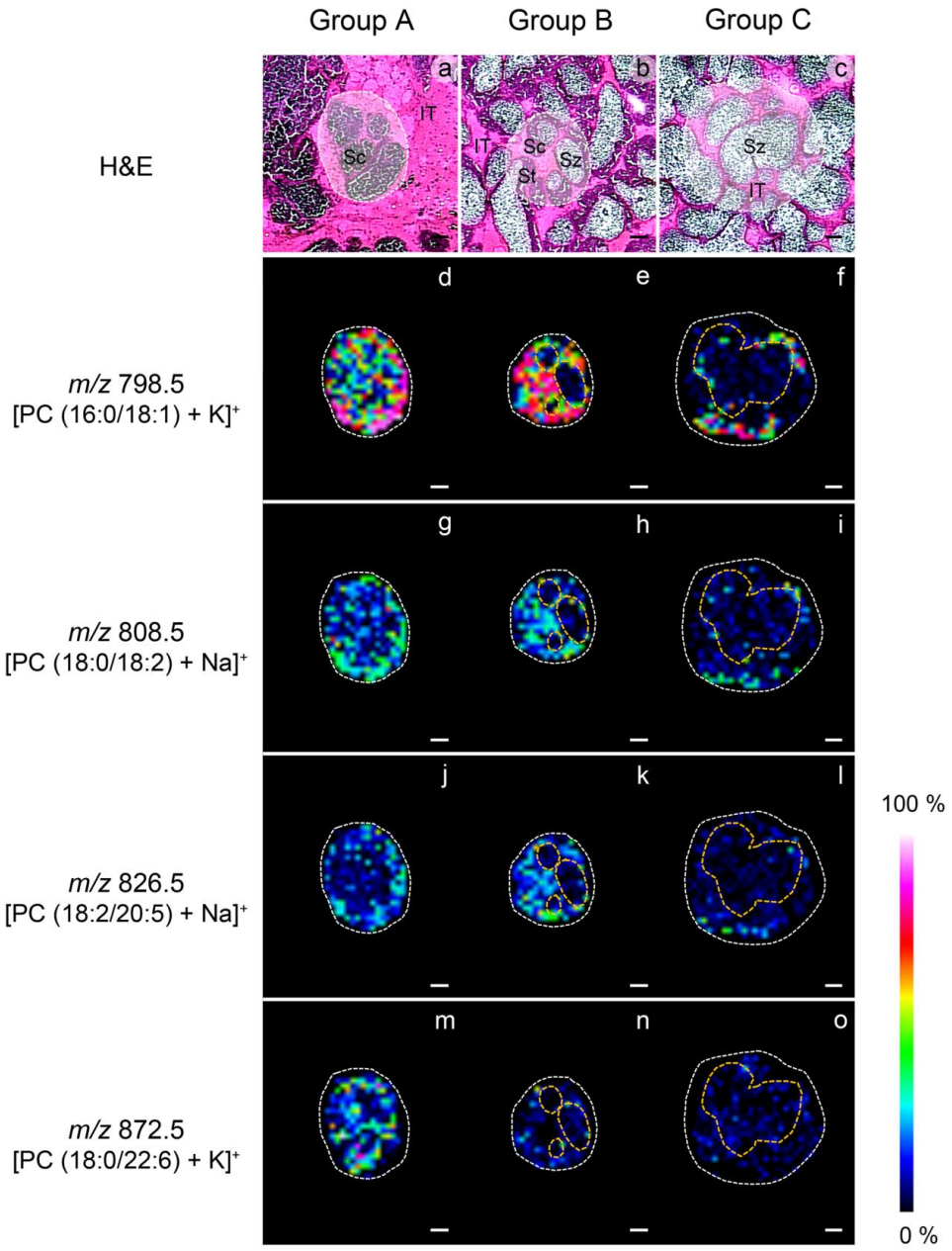

Figure 5.25 IMS showing the intensity and distribution of PCs in the STs of OC males at high magnifications. Micrographs from H&E-stained sections (a-c) show areas surrounded by white dashed lines corresponding to the same areas that display ion images (d-o). Sz = spermatozoa; Sc = spermatocytes; St = spermatids; IT = intertubular area; Scale bars = 200 μm; Relative intensity bar shows the intensity level of the ion image.

Table 5.3 MS/MS and IMS identifications and distributions of phosphatidylcholines (PCs) in three groups of seminiferous tubules (STs).

m/z	**FA composition**	**Adduct**	**Distribution in ST groups**
756.5	16:0/16:1	Na	--, B, C
760.5	16:0/18:1	H	A, B, C
780.5	16:0/18:2	Na	A, B, C
782.5	16:0/18:1	Na	A, B, C
784.5	16:0/18:0	Na	A, B, --
796.5	16:0/18:2	K	A, B, C
798.5	16:0/18:1	K	A, B, C
800.5	16:0/18:0	K	A, B, --
804.5	18:2/18:2	Na	A, B, C
806.5	18:1/18:2	Na	--, B, C
808.5	18:0/18:2	Na	A, B, --
810.5	18:0/18:1	Na	--, B, C
824.5	18:0/18:2	K	A, B, --

[a]--, not detected.

Table 5.4 Identification of phosphatidylcholines (PCs), containing arachidonic acid (ARA), eicosapentaenoic (EPA), and docosahexaenoic acid (DHA), and their distributions in the three groups of seminiferous tubules (STs).

m/z	FA composition	Adduct	Distribution in ST groups
820.5	16:0/20:4 **ARA**	K	A, B, --
826.5	18:2/20:5 **EPA**	Na	A, B, --
828.5	16:0/22:6 **DHA**	Na	A, --, --
830.5	18:1/20:4 **ARA**	Na	A, B, C
832.5	18:0/20:4 **ARA**	Na	A, --, --
844.5	16:0/22:6 **DHA**	K	A, --, --
846.5	18:0/20:5 **EPA**	K	A, B, --
870.5	18:1/22:6 **DHA**	K	A, --, --
872.5	18:0/22:6 **DHA**	K	A, --, --

All PC species, except those underlined in this table, were identified by MS/MS analysis, and their distributions determined by IMS. The underlined PCs were partial fragments identified by using Metabolite MS Search (http://www.hmdb.ca/labm/jsp/mlims/MSDbParent.jsp).

[a]--, not detected.

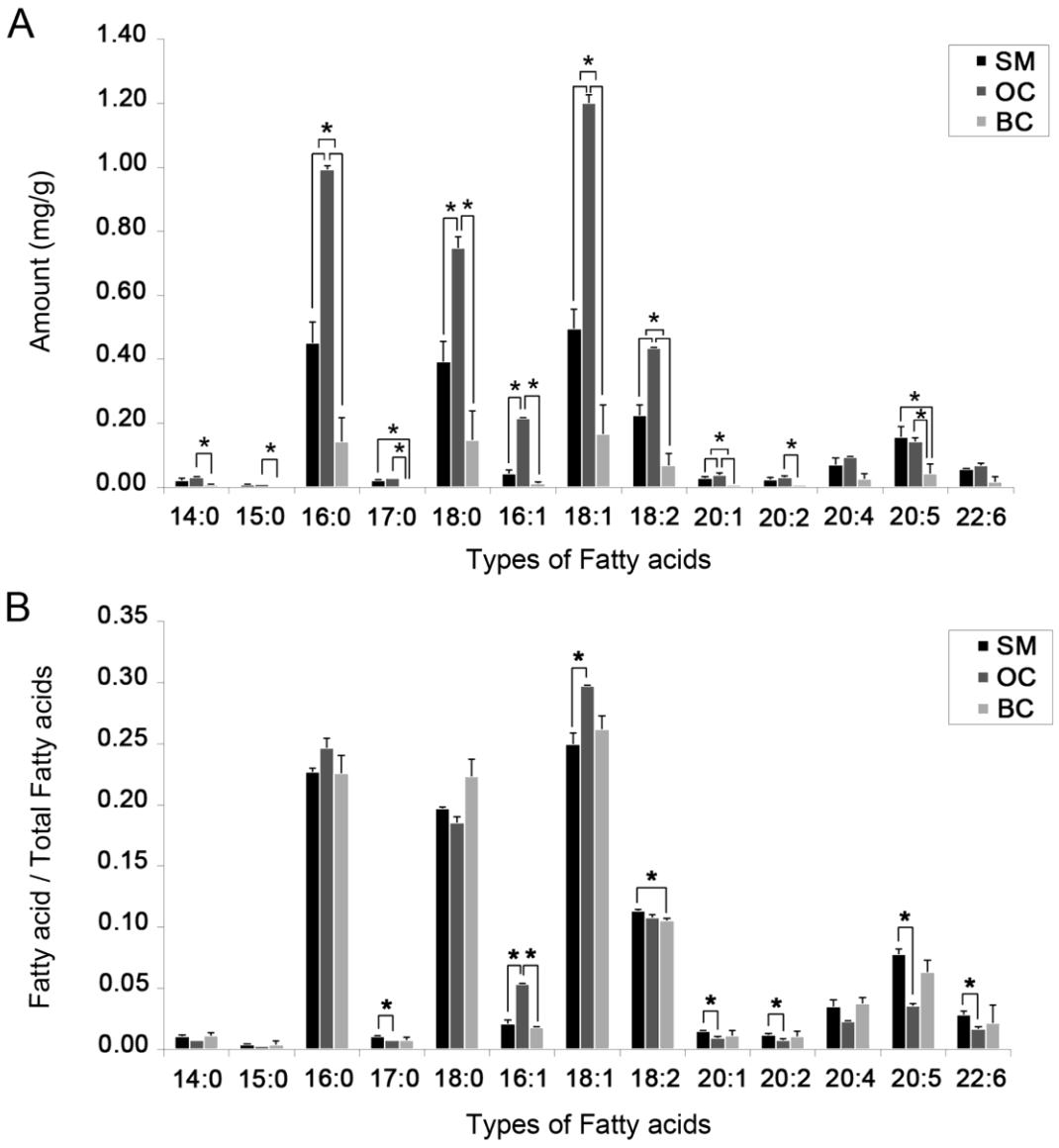

Figure 5.26 Gas Chromatography-mass spectrometry (GC-MS) analyses show (A) the amounts of FAs per testicular weight (mean ± SD; n = 5), and (B) the ratios between each FA per total FAs in the testes of the three developmental male morphotypes. 20:4 = ARA, Arachidonic acid; 20:5 = EPA, Eicosapentaenoic acid; 22:6 = DHA, Docosahexaenoic acid; SM = small male; OC = orange claw male; BC = blue claw male; * = significant difference at $P<0.05$.

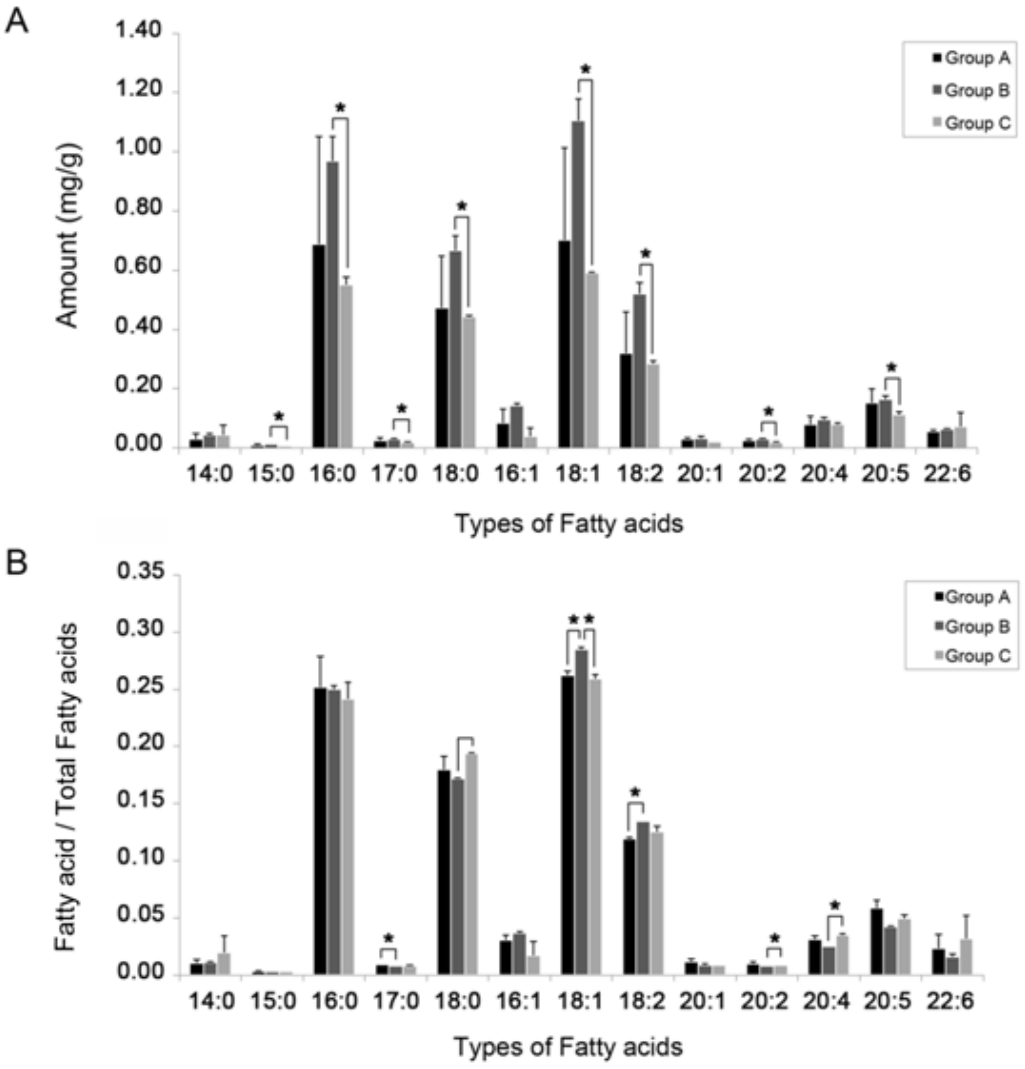

Figure 5.27 Gas Chromatography-mass spectrometry (GC-MS) analyses show (A) the amounts of FAs per testicular weight (mean ± SD; n = 5), and (B) the ratios between each FA per total FAs in the testes of the three group of STs. 20:4 = ARA, Arachidonic acid; 20:5 = EPA, Eicosapentaenoic acid; 22:6 = DHA, Docosahexaenoic acid; * = significant difference at $P<0.05$.